bioRxiv preprint doi: https://doi.org/10.1101/777979; this version posted November 7, 2019. The copyright holder for this preprint (which was not certified by peer review) is the author/funder. All rights reserved. No reuse allowed without permission.

Contribution of NPY Y_5 Receptors to the Reversible Structural Remodeling Of Basolateral Amygdala Dendrites in Male Rats Associated with NPY-mediated Stress Resilience.

Sheldon D. Michaelson[1], Ana Pamela Miranda Tapia[1], Amanda McKinty[1], Heika Silveira Villarroel[1], James P. Mackay[1], Janice H. Urban[2], William F. Colmers[1*]

[1] Department of Pharmacology, and the Neuroscience and Mental Health Institute, University of Alberta, Edmonton, Alberta, T6G 2H7, Canada
[2] Center for the Neurobiology of Stress Resilience and Psychiatic Disorders; Discipline of Physiology and Biophysics, Chicago Medical School, Rosalind Franklin University of Medicine and Science, North Chicago, IL, 60064 USA

***Corresponding Author:** Dr. William F. Colmers, Department of Pharmacology and Institute for Neuroscience and Mental Health, University of Alberta, 9-36 MSB, Edmonton, AB. T6G 2H7, Canada. wcolmers@ualberta.ca

Number of Figures:	13
Number of Tables :	2
Abstract:	244 words
Significance Statement	116 words
Introduction	648 words
Discussion	1486 words

Acknowledgments: We are grateful for the generous contributions of NPY receptor-selective agonists by Prof. Annette Beck-Sickinger, University of Leipzig. SDM received funding from Alberta Innovates Health Solutions (AIHS) (Doctoral studentship). JPM received Canadian Institute of Health Research (CIHR) (Doctoral and Masters studentships), and a Doctoral studentship from AIHS. WFC was a Medical Scientist of the Alberta Heritage Foundation for Medical Research for most of this period.
This work was supported by NIH grants MH081152 and MH090297 (to JHU & WFC), and support by the University of Alberta Hospitals Foundation to WFC.

Author Contributions: SDM, APMT, JHU and WFC designed experiments. SDM, APMT, AM, HSV and JM performed experiments. SDM, APMT and AM analyzed data. SDM, JHU and WFC wrote the manuscript. SDM and WFC conceived the study. All authors edited the manuscript.
Competing Interests: The authors declare no competing financial interests.
Running Header:NPY causes reversible changes in BLA dendrites

Data availability: The data that support the findings of this study are available from the corresponding author upon reasonable request.

bioRxiv preprint doi: https://doi.org/10.1101/777979; this version posted November 7, 2019. The copyright holder for this preprint (which was not certified by peer review) is the author/funder. All rights reserved. No reuse allowed without permission.

ABSTRACT

Endogenous neuropeptide Y (NPY) and corticotrophin-releasing factor (CRF) modulate the responses of the Basolateral amygdala (BLA) to stress, and are associated respectively with the development of stress resilience and vulnerability. We characterized the persistent effects of repeated NPY and CRF treatment on the structure and function of BLA principal neurons (PN) in a novel organotypic slice culture (OTC) model of rat BLA, and examined the contributions of specific NPY receptor subtypes to these neural and behavioral effects. In BLA principal neurons within the OTCs, repeated NPY treatment caused persistent attenuation of excitatory input and induced dendritic hypotrophy via Y_5 receptors; conversely, CRF increased excitatory input and induced hypertrophy of BLA PNs. Repeated treatment of OTCs with NPY followed by an identical treatment with CRF, or vice versa inhibited or reversed all structural changes in OTCs. These structural responses to NPY or CRF required calcineurin or CaMKII, respectively. Finally, repeated intra-BLA injections of NPY or a Y_5 receptor agonist increased social interaction and recapitulated structural changes in BLA neurons seen in OTCs, while a Y_5 receptor antagonist prevented NPY's effects both on behavior and on structure. These results implicate the Y_5 receptor in the long-term, anxiolytic-like effects of NPY in the BLA, consistent with an intrinsic role in stress buffering, and highlight a remarkable mechanism by which BLA neurons may adapt to different levels of stress. Moreover, BLA OTCs offer a robust model to study mechanisms associated with resilience and vulnerability to stress in BLA.

bioRxiv preprint doi: https://doi.org/10.1101/777979; this version posted November 7, 2019. The copyright holder for this preprint (which was not certified by peer review) is the author/funder. All rights reserved. No reuse allowed without permission.

Keywords: Organotypic slice cultures; Basolateral amygdala; Stress resilience; Neuropeptide Y; CRF, dendritic plasticity, Social interaction, NPY Y_5 receptor.

bioRxiv preprint doi: https://doi.org/10.1101/777979; this version posted November 7, 2019. The copyright holder for this preprint (which was not certified by peer review) is the author/funder. All rights reserved. No reuse allowed without permission.

Significance Statement: Within the basolateral amygdala (BLA), Neuropeptide Y (NPY) is associated with buffering the neural stress response induced by CRF, and promoting stress resilience. We used a novel organotypic slice culture (OTC) model of BLA, complemented with *in vivo* studies, to examine the cellular mechanisms associated with the actions of NPY. In OTCs, repeated NPY treatment reduces the complexity of the dendritic extent of anxiogenic BLA principal neurons, making them less excitable. NPY, via activation of Y5 receptors, additionally inhibits and reverses the increases in dendritic extent and excitability induced by the stress hormone, corticotropin releasing factor (CRF). This NPY-mediated neuroplasticity indicates that resilience or vulnerability to stress may thus involve neuropeptide-mediated dendritic remodeling in BLA PNs.

bioRxiv preprint doi: https://doi.org/10.1101/777979; this version posted November 7, 2019. The copyright holder for this preprint (which was not certified by peer review) is the author/funder. All rights reserved. No reuse allowed without permission.

INTRODUCTION

The stress response ensures survival through activation of a coordinated, adaptive response to perceived threats, which is terminated via neural and endocrine systems that buffer the stress and restore homeostasis. Failure to adequately terminate this response can result in abnormal neural responses which predisposes the individual to affective- and anxiety-related disorders (McEwen, 2003). The complex network of inhibitory and excitatory neurons in the amygdala, particularly the basolateral amygdala (BLA), integrates and processes stress-, emotion- and memory-related input (Phelps and Ledoux, 2005). Chronic or extreme stress can overwhelm this homeostatic control, resulting in an imbalance which enhances the excitatory, anxiogenic, output of BLA projection neurons (Roozendaal et al., 2009), partly through hypertrophy of dendritic arbors, including increased spine numbers (Mitra et al., 2005, Padival et al., 2013, Adamec et al., 2012, Hill et al., 2011, Vyas et al., 2002, 2006). These changes can persist for weeks (Vyas et al., 2004) and may underlie the development of stress-related psychiatric disease.

The endogenous neuropeptides corticotropin-releasing factor (CRF) and Neuropeptide Y (NPY) also regulate BLA activity, respectively increasing and inhibiting BLA output. CRF increases anxiety-like behavior (Rainnie et al., 2004; Sajdyk et al., 2004), while NPY has an important anxiolytic action in rodents (Sajdyk et al., 2002, 2004) and in humans, where NPY is also linked to resilience (Yehuda et al., 2006; Zhou et al., 2008). A balance between CRF and NPY activities within BLA is important for various behavioral responses (Sajdyk et al., 2004; Heilig 1994; 2004). Stress causes CRF release, which generates an appropriate behavioral response (e.g., freezing, fleeing); thereafter, these responses are buffered by NPY release, which curtails CRF actions and shortens

bioRxiv preprint doi: https://doi.org/10.1101/777979; this version posted November 7, 2019. The copyright holder for this preprint (which was not certified by peer review) is the author/funder. All rights reserved. No reuse allowed without permission.

the stress response (Heilig et al., 1994). An imbalance in either NPY or CRF tone can thus induce anxiolysis and anxiogenesis, respectively (Sajdyk et al., 2004, Heilig et al., 1994). Subjecting animals to either repeated stress (Padival et al, 2013) or daily injections of urocortin (UCN- a CRF-R1 and CRF-R2 agonist) induces anxiety that long outlasts the stimulus; conversely, a persistent (up to 2 months) stress resilience occurs with similar NPY treatment (Sajdyk et al,, 2008, Rainnie et al., 2004). These cellular responses likely underlie the ability of NPY to mitigate CRF- and stress-induced, BLA-mediated behaviors (Rainnie et al., 2004).

Acute cellular responses to NPY include hyperpolarization-induced inhibition of BLA PNs via suppression of the tonically active somatodendritic I_h; CRF excites these cells by activating their I_h (Giesbrecht et al., 2010). Moreover, NPY acutely decreases BLA activity by enhancing $GABA_A$-mediated inhibitory postsynaptic currents (IPSCs), and reducing NMDA-mediated excitatory postsynaptic currents (EPSCs) (Molosh et al., 2013) in BLA PNs. Using the model of NPY-induced resilience (Sajdyk et al., 2008), we recently showed that a reduction of I_h expression in BLA PNs contributes to, and mimics, long-term resilience (Silveira Villarroel et al., 2018), which we regard as the ability to rebound from trauma or severe stress (Yehuda, 2006). These acute anxiolytic actions of NPY are largely attributed to activation of the Y_1 receptor (Sajdyk et al., 2004).

While characterization of acute responses to NPY and CRF using *ex vivo* brain slices largely precludes easy interrogation of mechanisms underlying the persistent NPY and CRF effects on BLA neurons, organotypic slice cultures (OTCs) of hippocampus, spinal cord and cerebellum reliably model respective gross tissue organization, morphological, synaptic and neurochemical phenotypes (De Simoni et al., 2003, Lu et al., 2009, Gähwiler, 1981), and can be validated against

bioRxiv preprint doi: https://doi.org/10.1101/777979; this version posted November 7, 2019. The copyright holder for this preprint (which was not certified by peer review) is the author/funder. All rights reserved. No reuse allowed without permission.

acute preparations (e.g., De Simoni et al., 2003, Lu et al, 2009). OTCs also permit rigorous studies of chronic manipulations in a well-defined system (Humpel, 2015). Here we report OTC preparations of the BLA, a novel *in vitro* model of this stress-related circuitry, which reflects the *in vivo* effects of NPY and CRF, and predicts their mechanisms of action, including the reversible remodeling of PN dendritic structures. Moreover, this action was unexpectedly mediated *in vivo* and *in vitro* by activation of the Y_5 subtype receptor.

MATERIALS AND METHODS

Animals

All animal procedures were approved by the University of Alberta Animal Care and Use Committee: Health Sciences, in accordance with the guidelines of the Canadian Council on Animal Care. Litters of postnatal day (P) 14 and 5-week old male Sprague-Dawley rats, from the University of Alberta colony were used. P14 pups were given complete access to the dams for maternal care, then were removed from the dam just prior either to preparation of OTCs or for a subset of acute slice studies. Five-week-old rats were grouped housed (2-3 animals per cage) with 12:12 hours light:dark schedule and *ad libitum* access to food and water.

Development and validation of organotypic slice cultures (OTCs) of BLA

Postnatal development of the rat BLA continues until P28 (Ehrlich et al., 2012; 2013). Generation of OTCs from late adolescent or early adult-stage animals would be ideal, but the viability of OTCs declines steeply with postnatal age of origin (Humpel, 2015, Kim et al,, 2013). Our

bioRxiv preprint doi: https://doi.org/10.1101/777979; this version posted November 7, 2019. The copyright holder for this preprint (which was not certified by peer review) is the author/funder. All rights reserved. No reuse allowed without permission.

and others' previous work used larger (250 - 275g) Wistar or older (P42) Sprague-Dawley rats in studies of NPY and UCN effects on stress-resilience/vulnerability (), and acute and persistent NPY actions (Giesbrecht et al., 2010, Molosh et al., 2013, Silveira Villarroel et al., 2018).

OTC preparation

Organotypic cultures were prepared using the interface method described by Stoppini et al. (1991) with minor modifications. Briefly, P14 rats were decapitated and their brains rapidly removed under sterile conditions and submerged in ice-cold slicing solution [Hank's balanced salt solution (HBSS) + D-glucose (0.6 % final) + kynurenic acid (30 µM final)]. The brain was imbedded in agarose, and trimmed agarose-brain blocks were secured with cyanoacrylate glue to a custom slicing chamber, immersed in cold (<4ºC) slicing solution. Coronal slices (350 µm) were cut serially from rostral to caudal using a vibratome and trimmed to size. Four slices per hemisphere containing the BLA (as determined visually with a dissecting microscope), were allowed to rest in fresh slicing solution at 4°C for 30-45 minutes, and mounted on individual semiporous membrane inserts and placed in 24-well plates with 300 µL of culture media (50% Minimal Essential Medium (MEM), 25% heat-inactivated horse serum, 25% HBSS, supplemented with: 1 mM Glutamax, 1% D-glucose, 0.5 mM L-ascorbic acid, and 25 U/mL penicillin/streptomycin). After 48 hours in culture, an anti-mitotic solution of 1:1:1 cytosine-β-D-arabino-funanoside, uridine, and 5-Fluro-2'-deoxyuridine was added to the media (0.5 µM final concentration) for 24 hours to prevent glial proliferation. Slices were maintained at 37°C in 5%/95% CO_2/air. Media was changed three times per week for the duration of the experiment, except as indicated.

bioRxiv preprint doi: https://doi.org/10.1101/777979; this version posted November 7, 2019. The copyright holder for this preprint (which was not certified by peer review) is the author/funder. All rights reserved. No reuse allowed without permission.

BLA OTCs prepared from rats at P21 and P28 were poorly viable, but those from P14 (2 week) rats remained robustly viable to at least 8 weeks in culture, the equivalent postnatal (EP) age of P70 (**Fig. 1a**), permitting comparison of the electrophysiological and morphological properties of PNs from the OTCs (see below). Such OTCs were used for this entire study

OTC drug incubations

To mimic EP 6 weeks (4 weeks in culture), slices were treated with fresh media containing indicated concentrations of reagents, changed daily for five consecutive days; the last change remained until the normal Day 7 media change. When cultures were serially treated as above first with NPY then with CRF (or vice-versa), incubations proceeded with one peptide as above, followed with an identical one-week daily protocol using the opposing peptide starting with the Day 7 media change. A control subset of cultures was treated with the inactive desamido NPY analogue (daNPY – 100 nM). After incubations, media changes were again performed three times weekly (**Fig. 1a**).

Acute slice preparation

P14 or P70 rats were decapitated and their brains rapidly submerged in cold (4°C) artificial cerebrospinal fluid (aCSF) slicing solution, containing (in mM): 118 NaCl, 3 KCl, 1.3 $MgSO_4$, 1.4 NaH_2PO_4, 5.0 $MgCl_2$, 10 D-glucose, 26 $NaHCO_3$, 2.5 $CaCl_2$ and 1.0 kynurenic acid and bubbled with carbogen (95% O2, 5% CO_2) (Silveira Villarroel et al., 2018). Coronal sections (300 µm) containing the BLA were prepared using a vibrating slicer (HR2; Sigmann Elektronik, Hüffenhardt, Germany). Brain slices were then transferred to a room temperature (22°C), carbogenated aCSF containing

bioRxiv preprint doi: https://doi.org/10.1101/777979; this version posted November 7, 2019. The copyright holder for this preprint (which was not certified by peer review) is the author/funder. All rights reserved. No reuse allowed without permission.

the following (in mM): 124 NaCl, 3 KCl, 1.3 $MgSO_4$, 1.4 NaH_2PO_4, 10 D-glucose, 26 $NaHCO_3$, and 2.5 $CaCl_2$. Osmolality was adjusted to 300 mOsm/kg.

Comparison with PNs from acute slice preparations

PNs from BLA OTCs are morphologically complex and electrophysiologically more similar to PNs in acute slices from P70 than from P14 rats, though OTC neurons are considerably smaller than those from either acutely ex vivo (**Table 1**). Moreover, repeated NPY (100 nM) treatment of OTCs *in vitro* as illustrated in **Fig. 1a** increased the mean amplitude of spontaneous inhibitory postsynaptic currents (sIPSCs), while increasing the mean inter-event interval (IEI) of spontaneous excitatory postsynaptic currents (sEPSCs) (**Fig. 1b,c)**. In all, repeated NPY treatment (**Fig. 1b-e**) resulted in similar net increase in synaptic inhibition and reduction of synaptic excitation onto BLA PNs in OTCs as previously reported from *ex vivo* slices prepared from animals treated with NPY *in vivo* (Silveira-Villarroel, et al., 2018).

Stereotaxic surgery and intracranial injections

Stereotaxic surgery was carried out as described in detail elsewhere (Silveira Villarroel et al., 2018). Briefly, 5-week old animals were acclimatized to the animal facility and handled daily for 1 week prior to experimental manipulation. Rats were anesthetized with ketamine/xylazine (90:10 mg/kg) or with isoflurane using a SomnoSuite low flow vaporizer (Kent Scientific, Torrington, CT, USA) and placed in a stereotaxic apparatus (Kopf, Tujunga, CA, USA). Anaesthesia was monitored carefully to maintain surgical plane throughout, and animals were kept warm with a temperature-controlled blanket (Harvard Apparatus, Holliston MA, USA). Bilateral guide cannulas (26 gauge; Plastics One, Roanoke, VA, USA) were implanted to just above (2 mm) the BLA

bioRxiv preprint doi: https://doi.org/10.1101/777979; this version posted November 7, 2019. The copyright holder for this preprint (which was not certified by peer review) is the author/funder. All rights reserved. No reuse allowed without permission.

[anteroposterior (AP): -2.3; mediolateral (ML): ±5.0; dorsoventral (DV): -6.4; incisor bar: -3.2 mm] (Paxinos and Watson, 1986). The cannulas were secured to the skull with four stainless steel screws (2.8 mm; Plastics One, Roanoke, VA, USA) and self-curing acrylic resin (Lang Dental Manufacturing Company, Inc., IN, USA). After completion of surgery, all animals received meloxicam (Boerhringer Ingelheim, Burlington, Ontario, Canada; 1 mg/kg, s.c.), 1 ml of saline 0.9% s.c., and were placed in a warm environment until they had fully recovered from the anesthetic. Rats remained singly housed until they fully recovered from surgery, then were housed in pairs. Pairs were separated and animals housed singly one day prior to behavioral testing (below).

Intracranial injections

As reported elsewhere (Silveira Villarroel et al., 2018), all compounds were delivered bilaterally via 33 gauge injection cannulas (Plastics One) that extended 2 mm beyond the guide cannulas, using a dual-channel infusion pump (PHD ULTRA, Harvard Apparatus, Holliston, MA, USA). Vehicle (sterile saline) alone or containing drug(s) as described was delivered at 100 nL/30s per side; cannulae were left in place for 1 minute afterward to prevent backflow. All injections were performed once daily between 8:00 AM and 10:00 AM for successive 5 days. Animals were return to their home cage for 30 min following injections, then tested (if in their protocol) for social interaction (SI).

Behavioral testing

The SI test was performed according to Sajdyk et al., (2008), with minor modifications. Briefly, an experimental animal was placed into the SI box (96 cm long x 96 cm wide x 30 cm high with an open top) simultaneous with a partner rat of the same sex, age and weight, housed

bioRxiv preprint doi: https://doi.org/10.1101/777979; this version posted November 7, 2019. The copyright holder for this preprint (which was not certified by peer review) is the author/funder. All rights reserved. No reuse allowed without permission.

under identical conditions but which had not encountered the experimental animal previously. Seventy-two hours after implantation surgery, rats received a sham intra-BLA injection, then were placed in the behavioral testing arena for 10 minutes alone to acclimate. Twenty-four hours later they received another mock injection, and SI was observed for 10 minutes to establish baseline anxiety-like levels prior to any experimental manipulations. Two days later, rats received a bilateral intra-BLA injection (vehicle or drug) and were tested for SI 30 min later (day 1). Injections continued daily at the same time and the SI test was repeated 30 min after the fifth injection (day 5), then at 2 weeks and 4 weeks from the first injection. Behavior was video recorded and later analysed by individuals blinded to treatment.

Whole-cell patch clamp electrophysiology

Acutely prepared slices or EP 9-10 week OTC slices (with culture insert membrane still attached), were transferred to a fixed recording chamber beneath a movable upright microscope (Axioskop FS2; Carl Zeiss, Germany)(Giesbrecht et al., 2010, Silveira Villarroel et al., 2018). Slices were perfused at 2-3 mL/min for at least 10 minutes before recording, with warmed (32-34°C), carbogenated aSCF (300 mOsm/L acute slices and 320 mOsm/L for OTCs - adjusted with NaCl). Patch pipettes were pulled from borosilicate glass (TW150F; World Precision Instruments, Sarasota, FL, USA) with a two-stage puller (PP-83; Narishige, East Meadow, NY, USA) and had a resistance of 4-6 MΩ with an internal solution (mM): 126 K-gluconate, 4 KCl, 10 HEPES, 5 MgATP, 0.3 NaGTP, 1 EGTA, 0.3 $CaCl_2$ and 0.2% neurobiotin (pH 7.27, 275 mOsm/L for acute slices and 300 mOsm/L for OTCs).

bioRxiv preprint doi: https://doi.org/10.1101/777979; this version posted November 7, 2019. The copyright holder for this preprint (which was not certified by peer review) is the author/funder. All rights reserved. No reuse allowed without permission.

The BLA was identified under a 5x objective and PNs identified visually with infrared-differential interference contrast (60x) optics. Neurons were selected as previously reported (Giesbrecht et al., 2010, Silveira Villarroel et al., 2018) based on morphological and electrophysiological criteria. PNs chosen for study were in random locations throughout the BLA; 1-3 neurons per slice were studied. Either a Multiclamp 700B or AxoClamp2A amplifier was used together with a DigiData 1322 or Digidata 1440 interface and pCLAMP v10.4 software (all Molecular Devices, Sunnyvale CA, USA). Gigohm seal, whole-cell recordings were low-pass filtered at 2 kHz and digitized at 10 kHz. Access resistance was measured throughout the experiment, and only those cells with changes less than 20% were kept for further analysis. The membrane potential reported was corrected offline for the calculated 15 mV liquid junction potential (Silveira Villarroel et al., 2018, Chee et al., 2010). Recordings (> 20 min) were terminated by gradually withdrawing the pipette until the membrane re-sealed.

Capacitance was calculated offline with pClamp, from the area under the curve of the current amplitude from a 200 ms, 10 mV hyperpolarizing voltage step (Taylor, 2012). No capacitance compensation was applied during these measurements. Spontaneous synaptic activity was assessed in voltage clamp at a (liquid junction potential corrected) holding potential of -55 mV and sampled at 20 kHz.

Cell processing and labeling

Neurons from *ex vivo* and OTC slices were all processed, stained, imaged, reconstructed and subjected to the same morphological analyses. Following patch clamp recordings, OTCs and acute slices were fixed with 10 % formalin (Thermo Fisher Scientific, Ottawa, Ontario, Canada) for

bioRxiv preprint doi: https://doi.org/10.1101/777979; this version posted November 7, 2019. The copyright holder for this preprint (which was not certified by peer review) is the author/funder. All rights reserved. No reuse allowed without permission.

24-72 h at 4°C, and then transferred to 0.2% sodium azide in PBS for subsequent storage at 4°C. Slices were processed within 4 weeks following patch clamp recordings. Free-floating slices were washed for 3 x 10 min periods in PBS before blocking and permeabilization for 2 h with 0.3 % Triton X-100 in PBS and 4% normal goat serum (Sigma-Aldrich, Oakville, Ontario, Canada). Slices were incubated with streptavidin conjugated with Alexa Fluor 555 or 546 (1:1000; Life Technologies, Grand Island, New York, USA) in 0.3 % Triton X-100 in PBS with 4% normal goat serum for 3 h at room temperature. Slices were washed 4 x10 min each in PBS, mounted on Superfrost Plus slides and coverslips were applied with Prolong Gold mounting media (Thermo Fisher). Slides were allowed to air dry in the dark at room temperature before being imaged via confocal microscopy.

Imaging and neuronal reconstruction

For morphological analysis of filled neurons, z-stack images were obtained with a 20x objective, 1024 x 1024 resolution, 100 Hz, excitation wavelength 543 nm, for a series of 0.8 µm steps with a laser scanning confocal microscope (Leica TCS SP5; Leica Microsystems, Canada). To determine the position of each neuron within the slice, multiple single-plane images were taken at 10x magnification, 512 x 512 resolution and 100 Hz, and stitched together using Leica LAS AF software. Only those neurons whose dendritic arbor was clearly and completely filled and cell body was clearly within the boundaries of the BLA were used for analysis. Neuronal reconstruction was performed using the simple neurite tracer function in FIJI (NIH, Bethesda, MD, USA). Following tracing, Sholl analysis (Sholl, 1953) of the entire 3-dimensional dendritic arbor was performed with another FIJI software module using concentric circles with increasing radii of 10 µm to determine

bioRxiv preprint doi: https://doi.org/10.1101/777979; this version posted November 7, 2019. The copyright holder for this preprint (which was not certified by peer review) is the author/funder. All rights reserved. No reuse allowed without permission.

dendritic intersections vs. distance from the soma. Total dendritic length and dendritic branching was calculated using FIJI and Excel software. Quantification of dendritic spine density was achieved by manually counting dendritic spines in z-stack images taken at 100x magnification, 1024 x 1024 resolution and 100 Hz for a series of 0.5 um steps. Spines were counted on three separate, randomly selected, 100 µm dendrite segments for each neuron analysed in a treatment group. All protrusions that were connected to the dendrite segment were considered as spines, but were not categorized by spine morphologies. Total spine number was estimated from the average spine density and total dendritic length for an individual neuron. Experimenters were blinded to culture treatment at the time of reconstructions.

Reagents and Drugs

NPY (human, rat) was purchased from Polypeptide Group (San Diego, CA, USA) while CRF was obtained from Phoenix Pharmaceuticals Inc. (Burlingame, CA, USA). The Y_1-agonist (F^7,P^{34}-NPY), the Y_5-agonist ([cPP$^{1-7}$,NPY$^{19-32}$,Ala^{31},Aib^{32},Gln^{34}]hPP) and the Y_2 agonist ([ahx$^{5-24}$] NPY) were generous gifts from Dr. A.G. Beck-Sickinger (Leipzig, Germany), while the Y_5-antagonist, CGP71683, was purchased from Tocris Bioscience (Bristol, UK). Cyclosporine A and okadaic acid were gifts respectively from Drs. Shairaz Baksh and Charles Holmes (University of Alberta, Canada). The cell permeable CaMKII inhibitor, myristoylated-autocamtide-2- related inhibitory peptide, was obtained from Enzo Life Sciences, Inc (Farmingdale, NY, USA). Culture reagents were all obtained from Gibco, except for Cytosine–β-D-arabino-furanoside, Uridine and 5’Fluro-2’deoxyuridine, which were from Sigma-Aldrich Canada. Pipette solution reagents were all from Sigma-Aldrich, except for Na-GTP (Roche Diagnostics).

bioRxiv preprint doi: https://doi.org/10.1101/777979; this version posted November 7, 2019. The copyright holder for this preprint (which was not certified by peer review) is the author/funder. All rights reserved. No reuse allowed without permission.

Experimental Design and Statistical Analysis

Electrophysiological recordings were viewed offline using pCLAMP. Traces from electrophysiological recordings, statistical analysis and graphs were prepared using versions 5 – 8 of Prism software (GraphPad, San Diego, CA, USA) or SPSS (version 20 - IBM). Neuronal reconstruction and Sholl analysis was performed using modules of the FIJI software suite (National Institutes of Health). Unless otherwise stated, all data are represented as mean ± s.e.m. D'Agostino-Pearson omnibus normality test was applied to determine data distributions. One-way analysis of variance (ANOVA) with Tukey's post-hoc test or Kruskal-Wallis H tests with Dunn's post hoc test were used as indicated, to compare cell capacitance, total dendritic lengths, branch points and spine density/total spine estimates between treatments. For Sholl analysis, two-way repeated measures ANOVA were used with Tukey's post-hoc test for multiple comparisons. A Linear Mixed-Model was used for analysis of SI studies. Treatment and time (with interaction term) were used as fixed effects, while we used intercepts for subjects as random effects. For data in **Table 1**, one-way ANOVA with Tukey's post-hoc test for multiple comparisons was used. For sEPSC and sIPSC analyses, two-sided Student's t-test or Mann-Whitney U tests were performed when applicable. OTC cultures for any given experiment were obtained from at least 3 animals (typically more), with data acquired from 1-3 neurons per OTC. With the extent of time in culture, and minimal number of neurons recorded from per slice, we opted to treat each neuron as an independent observation for statistical analysis. The number of animals, cultures and neurons per experimental group are indicated in **Table 2**. No statistical test was used to predetermine sample sizes, but our sample sizes are similar to those previously reported in the field (Adamec et al., 2012, Silveira Villarroel et

bioRxiv preprint doi: https://doi.org/10.1101/777979; this version posted November 7, 2019. The copyright holder for this preprint (which was not certified by peer review) is the author/funder. All rights reserved. No reuse allowed without permission.

al., 2018, DeSimoni et al., 2003). All analyses were two-sided. Significance was set at P<0.05 (* *P*<0.05, ***P*<0.01, ****P*<0.001, *****P*<0.0001).

RESULTS

Repeated NPY and CRF treatments cause dendritic hypotrophy and hypertrophy, respectively, in OTC PNs

Repeated restraint stress induces lasting dendritic hypertrophy in BLA neurons (Padival et al., 2013). Whereas *in vivo* administration of the CRFR1 agonist, UCN into the BLA elicits long-term stress vulnerability, NPY administration persistently decreases the animals' vulnerability to stress (Sajdyk et al., 2008, Rainnie et al., 2004, Silveira Villarroel et al., 2018). The enduring effects of NPY may parallel the persistence of the stress-induced dendritic hypertrophy in BLA neurons (Padival et al., 2013), but mechanisms underlying the effects of either endogenous neuropeptide remain unclear. To test our hypothesis that repeated application of either NPY or CRF to BLA OTCs will alter electrophysiological properties of PNs and result in their respective hypotrophy or hypertrophy, we monitored PN properties with electrophysiology and post-recording morphological analysis. Initial validation of the OTC preparation of BLA (Material and Methods) included an extensive comparision of PN neuronal properties with neurons from acute *ex vivo* brain slices of P14 and P70 animals **(Table 1)**; the PNs from OTCs were more compact but electrically more similar to those from acute slices from the adult animals.

bioRxiv preprint doi: https://doi.org/10.1101/777979; this version posted November 7, 2019. The copyright holder for this preprint (which was not certified by peer review) is the author/funder. All rights reserved. No reuse allowed without permission.

Repeated application of NPY (1 – 100 nM) reduced PN whole-cell capacitance relative to vehicle controls (**Fig. 2a**). Consistent with this, NPY (≥ 1 nM) reduced and simplified the dendritic arbor (**Fig. 2b-j**), decreasing the total dendritic length (**Fig. 2b**) and complexity of dendritic branching (**Fig. 2c,d**). NPY's effects on dendritic morphology were already significant at 1 nM ($p < 0.0001$ vs. control). Although dendritic spine density was not altered by 100 nM NPY, estimates of total spine numbers showed a trend toward reduction compared to controls (**Fig. 3**), consistent with the significant reduction in EPSC frequencies observed (**Fig. 1b,c,e**). Neurons treated with the inactive, desamido NPY analogue (daNPY – 100 nM) (Wahlestedt et al., 1986), did not differ in any aspect from untreated controls (**Fig. 2a-d,f**).

Repeated treatment of OTCs with CRF induced a diametrically opposite set of changes in BLA PN physiology and structure. Thus, application of 30 nM CRF increased sEPSC frequency compared to vehicle-treated PNs (**Fig. 1 f-h**). Furthermore, compared with controls, CRF increased whole-cell capacitance (**Fig. 4a**) and caused hypertrophy of the dendritic arbor (**Fig. 4b**), including increased branching (**Fig. 4c**) and dendritic complexity (**Fig. 4d-g**). The effects of CRF on dendritic morphology occurred in a more clearly concentration-dependent manner than did those of NPY. Although CRF-treatment did not alter spine density, estimates of total spine numbers were significantly increased compared to controls (**Fig. 3**).

Bi-directional PN dendritic remodeling after successive treatments with NPY and CRF in BLA OTCs

BLA output, and thus the physiological and behavioral responses to stress are governed in part by the opposing actions of NPY and CRF neuropeptide systems. Disruption of this homeostatic

bioRxiv preprint doi: https://doi.org/10.1101/777979; this version posted November 7, 2019. The copyright holder for this preprint (which was not certified by peer review) is the author/funder. All rights reserved. No reuse allowed without permission.

mechanism may in part underlie some persistent anxiety-related disorders (Schmeltzer et al., 2016). We therefore next determined if NPY and CRF can also act as counter-regulatory signals in BLA OTCs. BLA OTCs were incubated for one week with either CRF or NPY, then some were incubated the following week respectively with either NPY or CRF, and maintained in control media for one additional week before electrophysiological and morphological analyses were performed on both single- and double-treated populations. Specifically, when PNs were reciprocally treated with the two peptides in either order, there were no differences either in cell capacitance (**Fig. 5a**) or dendritic size or complexity (**Fig. 5b-g**) from vehicle controls. As in the previous experiments, application of NPY or CRF alone either decreased or increased the frequency of sEPSCs observed in the OTCs, whereas sEPSC frequency in the CRF,NPY- or NPY,CRF-treated groups was not significantly different from vehicle controls (**Fig. 5h-k**). Assessment of BLA PN morphology in the CRF,NPY and NPY,CRF groups was consistent with the neurons undergoing a bi-directional structural plasticity.

The Y_5R but not the Y_1R mediates dendritic hypotrophy in BLA OTCs

While NPY plays a key role in behavioral stress resilience, the receptor subtype(s) mediating the long-term effect on behavior is unknown. The BLA expresses Y_1, Y_2 and Y_5 NPY receptors (Kopp et al., 2002; Wolak et al., 2003; Stanic et al., 2011) and while the acute anxiolytic effects of NPY in the BLA are mediated predominantly via the Y_1R (Sajdyk et al., 2002a), evidence also suggests a role for the Y_5R (Sajdyk et al., 2002a). Unexpectedly, selective activation of Y_2 receptors in the BLA acutely increases PN excitability (Mackay et al., 2019) and facilitates the

bioRxiv preprint doi: https://doi.org/10.1101/777979; this version posted November 7, 2019. The copyright holder for this preprint (which was not certified by peer review) is the author/funder. All rights reserved. No reuse allowed without permission.

anomalous expression of anxiety-like behaviors (Sajdyk et al., 2002b). We thus examined the roles of different NPY receptors in a pharmacological experiment using BLA OTCs.

In a repeated incubation experiment as with NPY above, the Y_1R-selective agonist, F^7,P^{34}-NPY (1–100 nM) had no measurable long-lasting effects on the properties of BLA OTC PNs compared to controls at any concentration tested. Thus, whole-cell capacitance (**Fig. 6a**), or any of the morphological parameters affected by NPY itself in this system were unchanged (**Fig. 6b-d**). Treatment with the Y_1R-selective agonist also had no significant effect on sEPSC frequency (**Fig. 7 a-c**). The Y_2R-selective agonist, [ahx$^{5-24}$]NPY (1 – 100 nM; Beck-Sickinger et al, 1992), when tested at 1nM and 10 nM had non-significant effects on the same parameters for the Y_1R agonist as above, but when applied at 100 nM, we observed a significant increase, relative to vehicle, both in whole-cell capacitance and in dendritic arborization (total dendritic length and number of branches; **Fig. 8a-g**) which was similar to that seen with CRF. These results are consistent with previously reported anxiogenic actions of Y_2 receptor agonists (Sajdyk et al, 2002a,b), and indicate the Y_2 receptor is unlikely to mediate NPY-induced hypotrophy.

Finally, we tested the Y_5R-selective agonist, [cPP$^{1-7}$,NPY$^{19-23}$,Aib^{32},Gln^{34}] hPP ("cPP" - Cabrele et al., 2001) (1–100 nM). At 100 nM, cPP caused significant reductions in PN sEPSC frequency and increased sIPSC frequency compared to controls, with no changes in sIPSC or sEPSC amplitude (**Fig. 7d-g**). Concentrations of cPP ≥ 10 nM also caused robust decreases in PN whole-cell capacitance (**Fig. 9a**), total dendritic length, and numbers of branch points (**Fig. 9b-g**). While spine density was not altered by 100 nM cPP, estimates of total spine numbers per neuron were significantly reduced when compared with vehicle controls (**Fig. 3**). Furthermore, co-incubation of

bioRxiv preprint doi: https://doi.org/10.1101/777979; this version posted November 7, 2019. The copyright holder for this preprint (which was not certified by peer review) is the author/funder. All rights reserved. No reuse allowed without permission.

the Y_5R antagonist, CGP71683A (CGP, 30 nM) with a maximally effective concentration (30 nM) of NPY not only prevented NPY effects on whole-cell capacitance and dendritic extent, but actually caused dendritic hypertrophy (**Fig. 9a-g**). This effect is consistent with the Y_5 antagonist unmasking the Y_2-mediated actions of NPY reported above.

***In vivo* treatment of BLA with NPY or cPP results both in long-term behavioral stress resilience and dendritic hypotrophy**

Based on the *in vitro* results, we hypothesized that NPY will cause similar effects on PN structure in BLA *in vivo*, and that the structural changes would also correlate with persistent increases in social interaction, a validated measure of anxiety (File and Seth, 2003, Silveira Villarroel et al, 2018), which permits repeated longitudinal measures in individual animals, unlike many other paradigms such as the elevated plus maze. Five sequential daily injections either of NPY (10 pmol/100 nL), the Y_1-agonist F^7P^{34}NPY (10 pmol/100 nL), the Y_5-agonist, cPP (10 pmol/100 nL), or NPY co-applied with the Y_5-antagonist CGP (each 10 pmol/100 nL) were administered bilaterally into BLA of 8 week-old male rats. All NPY agonist treatments in this experiment acutely increased social interaction (SI) on injection days one and five relative both to pre-treatment baseline and to vehicle controls (**Fig. 10a**). However, only animals treated with NPY or the Y_5-agonist retained this increase in SI at 2 and 4 weeks (**Fig. 10a**). In recordings from PNs in acute *ex vivo* BLA slices from these same animals at 4 weeks post-treatment, prior treatment with either NPY or the Y_5R agonist decreased whole-cell capacitance (**Fig. 10b)** and significantly reduced dendritic extent and complexity relative to PNs from the vehicle-treated animals (**Fig. 10c-j**). Co-administration of the Y_5R antagonist with NPY prevented the long-term effects of NPY both on

bioRxiv preprint doi: https://doi.org/10.1101/777979; this version posted November 7, 2019. The copyright holder for this preprint (which was not certified by peer review) is the author/funder. All rights reserved. No reuse allowed without permission.

behavior and PN morphology (**Fig. 10a-e, j**); no anxiogenic behavior was observed at any timepoint, nor were increases in PN capacitance or arborization as seen in the OTCs. Therefore, the Y_5R is both necessary and sufficient to mediate both the NPY-induced long term structural plasticity and decreased behavioral stress responses *in vivo*.

Dendritic remodeling by NPY or CRF requires calcineurin or CaMKII, respectively

Because the long term stress -vulnerability and -resilience effects of CRF- and NPY-receptors are mediated via CaMKII- and calcineurin, respectively in the BLA *in vivo* (Rainnie et al., 2004, Sajdyk et al., 2008,), we hypothesized that the effects of NPY or CRF on BLA PN dendritic structure require the actions of calcineurin or CaMKII activity, respectively. We first repeatedly incubated BLA OTCs with NPY (10 nM) together with cyclosporin A (CsA, 2 µM), a protein phosphatase (PP) inhibitor which blocks calcineurin (Liu et al, 1991). Addition of CsA inhibited NPY-mediated dendritic hypotrophy and decreases in capacitance (**Fig. 11a-d**), resulting instead in PN dendritic hypertrophy, possibly by unmasking a Y_2R activation (**Fig. 11b-d**). While these results are consistent with a role for calcineurin, CsA is a general PP inhibitor and is not selective for calcineurin (PP2b). Okadaic acid (OA) selectively inhibits both PP1 and PP2a but not calcineurin (Cohen et al., 1990). Treatment of the BLA OTCs with the Y_5-agonist cPP (100 nM) in the presence of OA (10 nM) did not alter the effects of the Y_5R agonist on either capacitance or dendritic morphology, consistent with a specific role for calcineurin not only in NPY-mediated anxiolysis (Sajdyk et al., 2008) but also in NPY-mediated PN dendritic hypotrophy (**Fig. 11a-d**).

We then tested the role of CaMKII in mediating the hypertrophic actions of CRF in BLA OTC PNs by using a cell-permeant CaMKII inhibitor, the myristoylated version of autocamtide-2-related

bioRxiv preprint doi: https://doi.org/10.1101/777979; this version posted November 7, 2019. The copyright holder for this preprint (which was not certified by peer review) is the author/funder. All rights reserved. No reuse allowed without permission.

inhibitory peptide (AIP –Ishida et al., 1995). Inhibiting CaMKII activity with AIP (40 nM) prevented the CRF-mediated (30 nM) increase in cell capacitance and dendritic hypertrophy (**Fig. 11e-h**). This is consistent with a role for CaMKII in CRF-mediated dendritic hypertrophy and the resultant stress vulnerability generated by repeated stress and CRF-receptor activation (Rainnie et al., 2004).

DISCUSSION

Unraveling mechanisms mediating adaptive and pathophysiological responses to stress is key to developing treatments for stress-related disorders. The countervailing actions of CRF and NPY on BLA PNs represent a suite of mechanisms contributing to adaptive stress responses in the amygdala. Although both neuropeptides induce long-term neural changes linked to the initiation or mitigation of stress responses, the mechanisms underlying the effects of these neuropeptides are unclear. Here, we identify three novel and important insights into the function of NPY and CRF in amygdala physiology. First, we found that NPY-induced stress resilience ultimately involves a novel, persistent form of homeostatic plasticity, specifically, the reversible remodeling of dendritic structure in BLA pyramidal output neurons mediated by the Y_5R, which counterbalances the persistent hypertrophy seen with stress or repeated CRF-receptor activation. Second, different NPY receptors play nuanced and complex roles in the short-and long-term regulation of BLA excitability, structure and behavior. Finally, the BLA OTC preparation is a robust *in vitro* model, that mimics and predicts long-term in vivo responses of BLA neurons.

If the bidirectional changes in dendritic structure seen here with repeated neuropeptide treatments *in vitro* or *in vivo* are indeed biologically relevant, then intermittent but prolonged

bioRxiv preprint doi: https://doi.org/10.1101/777979; this version posted November 7, 2019. The copyright holder for this preprint (which was not certified by peer review) is the author/funder. All rights reserved. No reuse allowed without permission.

periods of stress should result in similar changes that can be reversed when conditions improve. Indeed, chronic stress or UCN treatment cause dendritic hypertrophy and increase excitatory inputs to BLA PNs (Padival et al., 2013, Rainnie et al., 2004); these increases in dendritic length and spine number are associated with enhanced excitatory drive onto BLA PNs, which increases anxiety (Mitra et al., 2005, Padival et al., 2013, Adamec et al., 2012, Hill et al., 2011, Vyas et al., 2002; 2006). While there is no simple behavioral manipulation to reverse the effects of prolonged stresses, repeated intra-BLA administration of NPY in vivo decreases the overall excitability of BLA PNs (Silveira Villarroel et al., 2018), and here we demonstrate similar effects of NPY on PNs both in BLA OTCs and in vivo, consistent with such a role for NPY. Moreover, the ability of NPY to constrain or reverse CRF's actions and vice-versa suggests a symmetrical regulation of PN dendritic properties. Following repeated NPY or CRF treatment, PNs in BLA OTCs also demonstrated respective decreases and increases in sEPSC frequencies, consistent with their respective behavioral effects. NPY and CRF thus appear to act via multiple, parallel mechanisms to mediate their opposing forms of plasticity, which when combined, drive BLA PN structure toward a resting state similar to that of naïve BLA. Consistent with a key role in stress homeostasis, NPY is thus poised to restore balance to the organism once a threat has dissipated. Future experiments employing either optogenetically or chemogenetically-induced activation of NPY neurons innervating BLA could test this hypothesis unambiguously.

The predominant role of the Y_5R in driving the long-term effects on BLA physiology and behavior was unanticipated. The Y_1R, which to date has received considerable attention in stress-

bioRxiv preprint doi: https://doi.org/10.1101/777979; this version posted November 7, 2019. The copyright holder for this preprint (which was not certified by peer review) is the author/funder. All rights reserved. No reuse allowed without permission.

mitigation, contributes only to the acute actions of NPY on SI behavior and fear extinction (Giesbrecht et al., 2010, Gutman et al., 2008). Because all NPY receptors couple to $G_{i/o}$ proteins (Michel et al., 1998), the different roles played by these two receptors might result from independent trafficking into separate signaling compartments within BLA neurons (Marley et al., 2013). Moreover, while the Y_1R desensitizes in somatic cell lines (Berglund et al., 2003) and intact systems (Holliday et al., 2005), evidence indicates that the Y_5R does not desensitize (Böhme et al., 2008). This potentially significant difference suggests that the Y_5R is more likely to be available for lasting mitigation of stress responses.

The long-term effects of NPY or CRF require the respective activation of the Ca^{2+}-dependent enzymes calcineurin and CaMKII, indicating a critical role for alterations in intracellular Ca^{2+} levels in BLA PNs as demonstrated both *in vivo* (Sajdyk et al., 2008, Rainnie et al., 2004) and now here in BLA OTCs. The acute and long-term enhancement of excitability caused by CRF would result in robust elevations in intracellular Ca^{2+} ($[Ca^{2+}]_i$), consistent with CaMKII activation requirements (Rainnie et al., 2004). However, how NPY achieves the more modest $[Ca^{2+}]_i$ elevation needed by calcineurin is less obvious. In this context, the differential contributions of the multiple NPY receptor subtypes within the BLA may provide some insight. Acute activation of BLA Y_2Rs paradoxically results in anxiogenic behavioral responses (Sajdyk et al., 2004a; 2004b), and resulted in CRF-like changes in BLA OTC neurons here. In both rat and mouse BLA, the Y_2R agonist reduces tonic $GABA_BR$ activation in BLA PNs by a presynaptically-mediated reduction in dendritic GABA release. This causes an increase in dendritic excitability and a disinhibition of dendritic Ca^{2+} channels, which in turn permits a moderately elevated Ca^{2+} influx in about half of BLA PNs (Mackay et al., 2019). These effects suggest that NPY release in BLA activates all 3 NPY receptors: Y_1Rs,

bioRxiv preprint doi: https://doi.org/10.1101/777979; this version posted November 7, 2019. The copyright holder for this preprint (which was not certified by peer review) is the author/funder. All rights reserved. No reuse allowed without permission.

which acutely hyperpolarize BLA PNs, Y_2Rs, which reduce dendritic $GABA_B$R activation and Y_5Rs, whose long-term effects rely on the preferential activation of calcineurin. In this scenario, the actions of the 3 separate NPY receptors would synergize to faciliate the Y_5R effect by modestly elevating Ca^{2+} influx into BLA PNs (**Fig. 12a)** while preventing the larger increases in $[Ca^{2+}]_i$ that would preferentially activate the CaMKII pathway favored by the CRF system (**Fig. 12b**). This model could in part also explain the greater potency of the pan-agonist NPY to affect dendritic structure. Nonetheless, further work is needed to more completely understand the pathways and mechanisms involved in this long-term structural plasticity.

Regulation of cytosolic protein phosphorylation plays a key role in the structural plasticity seen here, consistent with evidence that calcineurin and CaMKII act as downstream targets of anxiolytic and anxiogenic molecules in the BLA (Rainnie et al., 2004, Mineur et al., 2014, Lin et al., 2003). Both enzymes are inherently associated with synaptic plasticity in the BLA, so CRF- and NPY-mediated alterations in dendritic structure might also engage mechanisms that underlie LTP (long term potentiation) and LTD (long term depression), respectively (Pape and Pare, 2010). As LTP and LTD each require different levels of $[Ca^{2+}]_i$, studies on intra-dendritic Ca^{2+} dynamics could address the contributions made by acute or chronic changes in Ca^{2+} influx, either via NMDA receptors (Rainnie et al., 2004) or voltage-dependent Ca^{2+} channels, to dendritic remodeling (Pape and Pare, 2010).

Total dendritic length and whole-cell capacitance were tightly correlated in BLA OTC PNs over a variety of treatments (**Fig. 13**), were seen in BLA both *in vitro* and *in vivo*, and corresponded with long-term behavioral changes. Despite the potent acute behavioral effects of Y_1R agonists,

bioRxiv preprint doi: https://doi.org/10.1101/777979; this version posted November 7, 2019. The copyright holder for this preprint (which was not certified by peer review) is the author/funder. All rights reserved. No reuse allowed without permission.

they altered neither dendritic structure nor long-term behavior. It appears reasonable to speculate that structural changes mediated by repeated peptide treatments result in the long-term changes in behavioral response to stressors. In any case, this structural plasticity could provide a novel *in vitro* bioassay predicting efficacy of drug candidates.

OTCs have proved useful in the study of longer-term nervous system changes such as synaptic plasticity (Debanne et al., 1999, Selcher et al., 2012), and those associated with pathologies such as chronic pain (Lu et al., 2006), or even prion disorders (Campeau et al., 2013). Since such changes can involve alterations not only in synaptic microanatomy but also more robust changes in cellular architecture, the preservation of anatomical relations within the OTC is a distinct advantage. Mature PNs in BLA OTCs share more electrophysiological attributes with those in age-matched (10W) *ex vivo* BLA than those in *ex vivo* P14 rats, despite their increased compactness compared with neurons from either *ex vivo* preparation. Capacitance values were smaller, I_h activation kinetics (tau_{fast} and tau_{slow}) were faster, and sEPSC and sIPSC amplitudes were larger in BLA OTCs compared with the acute *ex vivo* neurons **(Table 1**). However, the properties of BLA OTC PNs as indicated by action potential properties, firing rates and AHPs suggests that growth within OTCs constrains the physical extent of otherwise physiologically mature OTC neurons.

In summary, we report a novel, readily and completely reversible alteration in PN dendritic structure that accompanies the long-term increase in behavioral stress resilience caused by NPY in the BLA, the mirror opposite of equivalent CRF actions. This action is unexpectedly mediated by the Y_5R, considered up to now a relatively minor player in mediating NPY's actions. These robust

bioRxiv preprint doi: https://doi.org/10.1101/777979; this version posted November 7, 2019. The copyright holder for this preprint (which was not certified by peer review) is the author/funder. All rights reserved. No reuse allowed without permission.

changes are readily observed in BLA OTCs, and are reflected nearly perfectly *in vivo*. Interestingly, the short- and longer-term actions of NPY are mediated by 3 different receptors, acting at 3 different targets to induce complex and comprehensive changes in postsynaptic properties and presynaptic connections in BLA PNs. The acute and longer-term actions both of NPY and CRF involve regulation of the same elements of the PN (I_h, dendrites, synaptic inputs), changes that correlate with, and in some cases (I_h) determine alterations both in excitability and behavior. The coordinated, countervailing regulation of these PN properties by NPY and CRF suggests other signals could access this machinery to regulate stress responses mediated by the BLA.

bioRxiv preprint doi: https://doi.org/10.1101/777979; this version posted November 7, 2019. The copyright holder for this preprint (which was not certified by peer review) is the author/funder. All rights reserved. No reuse allowed without permission.

References

Adamec, R., Hebert, M., Blundell, J. and Mervis, R.F. (2012). Dendritic morphology of amygdala and hippocampal neurons in more and less predator stress responsive rats and more and less spontaneously anxious handled controls. Behav. Brain Res. 226, 133-146.

Beck-Sickinger AG, Grouzmann E, Hoffmann E, Gaida W, van Meir EG, Waeber B, Jung G. (1992). A novel cyclic analog of neuropeptide Y specific for the Y2 receptor. Eur. J. Biochem. 206:957-964.

Berglund, M.M., Schober, D.A., Statnick, M.A., McDonald, P.H. and Gehlert, D.R. (2003). The use of bioluminescence resonance energy transfer 2 to study neuropeptide Y receptor agonist-induced beta-arrestin 2 interaction. J. Pharmacol. Exp. Ther. 306, 147-156.

Böhme I, Stichel J, Walther C, Mörl K, Beck-Sickinger AG.(2008). Agonist induced receptor internalization of neuropeptide Y receptor subtypes depends on third intracellular loop and C-terminus. Cell Signal. 20:1740-1749

Cabrele, C. and Beck-Sickinger, A.G. (2000). Molecular characterization of the ligand-receptor interaction of the neuropeptide Y family. J Pept Sci 6, 97-122.

bioRxiv preprint doi: https://doi.org/10.1101/777979; this version posted November 7, 2019. The copyright holder for this preprint (which was not certified by peer review) is the author/funder. All rights reserved. No reuse allowed without permission.

Cabrele, C., Wieland, H.A., Langer, M., Stidsen, C.E. and Beck-Sickinger, A.G. (2001). Y-receptor affinity modulation by the design of pancreatic polypeptide/neuropeptide Y chimera led to Y(5)-receptor ligands with picomolar affinity. Peptides 22, 365-378.

Campeau, J.L., Wu, G., Bell, J.R., Rasmussen, J. and Sim, V.L.(2013). Early increase and late decrease of purkinje cell dendritic spine density in prion-infected organotypic mouse cerebellar cultures. PLoS One 8, e81776.

Chee, M.J., Myers, M.G., Jr., Price, C.J. and Colmers, W.F. (2010). Neuropeptide Y suppresses anorexigenic output from the ventromedial nucleus of the hypothalamus. J. Neurosci. 30, 3380-3390.

Cohen P., Holmes, C.F., Tsukitani, Y. (1990) Okadaic acid: a new probe for the study of cellular regulation. Trends Biochem Sci. 15:98-102.

De Simoni, A., Griesinger, C.B. and Edwards, F.A. (2003) Development of rat CA1 neurones in acute versus organotypic slices: role of experience in synaptic morphology and activity. J. Physiol. 550, 135-147.

Debanne, D., Gahwiler, B.H. and Thompson, S.M. (1999). Heterogeneity of synaptic plasticity at unitary CA3-CA1 and CA3-CA3 connections in rat hippocampal slice cultures. J. Neurosci. 19, 10664-10671.

bioRxiv preprint doi: https://doi.org/10.1101/777979; this version posted November 7, 2019. The copyright holder for this preprint (which was not certified by peer review) is the author/funder. All rights reserved. No reuse allowed without permission.

Ehrlich, D.E., Ryan, S.J. and Rainnie, D.G. (2012). Postnatal development of electrophysiological properties of principal neurons in the rat basolateral amygdala. J. Physiol. 590, 4819-4838.

Ehrlich, D.E., Ryan, S.J., Hazra, R., Guo, J.D. and Rainnie, D.G. (2013). Postnatal maturation of GABAergic transmission in the rat basolateral amygdala. J. Neurophysiol. 110, 926-941.

File S.E. and Seth, P. (2003). A review of 25 years of the social interaction test. Eur J Pharmacol. 463:35-536.

Gahwiler, B.H. (1981). Morphological differentiation of nerve cells in thin organotypic cultures derived from rat hippocampus and cerebellum. Proc. R. Soc. Lond. B. Biol. Sci. 211, 287-290.

Giesbrecht, C.J., Mackay, J.P., Silveira, H.B., Urban, J.H. and Colmers, W.F. (2010) Countervailing modulation of Ih by neuropeptide Y and corticotrophin-releasing factor in basolateral amygdala as a possible mechanism for their effects on stress-related behaviors. J. Neurosci. 30, 16970-16982.

Gutman, A.R., Yang, Y., Ressler, K.J. and Davis, M. (2008). The role of neuropeptide Y in the expression and extinction of fear-potentiated startle. J. Neurosci. 28, 12682-12690.

bioRxiv preprint doi: https://doi.org/10.1101/777979; this version posted November 7, 2019. The copyright holder for this preprint (which was not certified by peer review) is the author/funder. All rights reserved. No reuse allowed without permission.

Heilig, M., Koob, G.F., Ekman, R. and Britton, K.T. (1994). Corticotropin-releasing factor and neuropeptide Y: role in emotional integration. Trends Neurosci. 17, 80-85.

Hill, M.N., Hillard, C.J. and McEwen, B.S. (2011). Alterations in corticolimbic dendritic morphology and emotional behavior in cannabinoid CB1 receptor-deficient mice parallel the effects of chronic stress. Cereb. Cortex 21, 2056-2064.

Holliday, N.D., Lam, C.W., Tough, I.R. and Cox, H.M. (2005). Role of the C terminus in neuropeptide Y Y1 receptor desensitization and internalization. Mol. Pharmacol. 67, 655-664.

Humpel, C. (2015). Organotypic brain slice cultures: A review. Neuroscience 305, 86-98.

Ishida, A., Kameshita, I., Okuno, S., Kitani, T. and Fujisawa, H. (1995). A novel highly specific and potent inhibitor of calmodulin-dependent protein kinase II. Biochem. Biophys. Res. Commun. 212, 806-812.

Kim, H., Kim, E., Park, M., Lee, E. and Namkoong, K. (2013) Organotypic hippocampal slice culture from the adult mouse brain: a versatile tool for translational neuropsychopharmacology. Prog. Neuropsychopharmacol. Biol. Psychiatry 41, 36-43.

Lin, CH, Yeh SH, Leu TH, Chang WC, Wang ST and Gean PW. (2003). Identification of calcineurin as a key signal in the extinction of fear memory. J. Neurosci. 23, 1574-1579.

bioRxiv preprint doi: https://doi.org/10.1101/777979; this version posted November 7, 2019. The copyright holder for this preprint (which was not certified by peer review) is the author/funder. All rights reserved. No reuse allowed without permission.

Liu, J., Farmer JD Jr, Lane WS, Friedman J, Weissman I and Schreiber SL. (1991). Calcineurin is a common target of cyclophilin-cyclosporin A and FKBP-FK506 complexes. Cell 66, 807-815.

Lu, V.B., Colmers, W.F. and Smith, P.A.(2009). Long-term effects of brain-derived neurotrophic factor on the frequency of inhibitory synaptic events in the rat superficial dorsal horn. Neuroscience 161, 1135-1143.

Lu, V.B., Moran TD, Balasubramanyan S, Alier KA, Dryden WF, Colmers WF and Smith PA. (2006). Substantia Gelatinosa neurons in defined-medium organotypic slice culture are similar to those in acute slices from young adult rats. Pain 121, 261-275.

Mackay, J.P., Bompolaki M, DeJoseph MR, Michaelson SD, Urban JH and Colmers WF. (2019). NPY2 Receptors Reduce Tonic Action Potential-Independent GABAB Currents in the Basolateral Amygdala. J. Neurosci. 39:4909-4930.

Marley, A., Choy, R.W. and von Zastrow, M. (2013). GPR88 reveals a discrete function of primary cilia as selective insulators of GPCR cross-talk. PLoS One 8, e70857.

McDonald, A.J. (1985). Immunohistochemical identification of gamma-aminobutyric acid-containing neurons in the rat basolateral amygdala. *Neurosci. Lett.* **53**, 203-207.

bioRxiv preprint doi: https://doi.org/10.1101/777979; this version posted November 7, 2019. The copyright holder for this preprint (which was not certified by peer review) is the author/funder. All rights reserved. No reuse allowed without permission.

McDonald, A.J., Beitz AJ, Larson AA, Kuriyama R, Sellitto C and Madl JE. (1989). Co-localization of glutamate and tubulin in putative excitatory neurons of the hippocampus and amygdala: an immunohistochemical study using monoclonal antibodies. *Neuroscience* **30**, 405-421.

McEwen, B.S. (2003). Mood disorders and allostatic load. *Biol. Psychiatry* **54**, 200-207.

Michel, M.C., Beck-Sickinger A, Cox H, Doods HN, Herzog H, Larhammar D, Quirion R, Schwartz T and Westfall T. (1989). XVI. International Union of Pharmacology recommendations for the nomenclature of neuropeptide Y, peptide YY, and pancreatic polypeptide receptors. Pharmacol. Rev. 50, 143-150.

Mineur, Y.S., Taylor, S.R. and Picciotto, M.R. (2014). Calcineurin downregulation in the amygdala is sufficient to induce anxiety-like and depression-like behaviors in C57BL/6J male mice. Biol. Psychiatry 75, 991-998.

Mitra, R., Jadhav, S., McEwen, B.S., Vyas, A. and Chattarji, S. (2005) Stress duration modulates the spatiotemporal patterns of spine formation in the basolateral amygdala. *Proc. Natl. Acad. Sci. U. S. A.* **102**, 9371-9376.

Molosh, A.I., Sajdyk TJ, Truitt WA, Zhu W, Oxford GS and Shekhar A. (2013). NPY Y1 receptors differentially modulate GABAA and NMDA receptors via divergent signal-transduction pathways to reduce excitability of amygdala neurons. Neuropsychopharmacology 38, 1352-1364.

bioRxiv preprint doi: https://doi.org/10.1101/777979; this version posted November 7, 2019. The copyright holder for this preprint (which was not certified by peer review) is the author/funder. All rights reserved. No reuse allowed without permission.

Padival, M.A., Blume, S.R. and Rosenkranz, J.A. (2013) Repeated restraint stress exerts different impact on structure of neurons in the lateral and basal nuclei of the amygdala. Neuroscience 246, 230-242.

Pape, H.C. and Pare, D. (2010). Plastic synaptic networks of the amygdala for the acquisition, expression, and extinction of conditioned fear. Physiol. Rev. 90, 419-463.

Paxinos, G. and Watson, C. (1986). The rat brain in stereotaxic coordinates (Academic Press, Sydney;

Phelps, E.A. and LeDoux, J.E. (2005). Contributions of the amygdala to emotion processing: from animal models to human behavior. Neuron 48, 175-187.

Rainnie, D.G., Bergeron R., Sajdyk T., Patil M., Gehlert D. and Shekhar A. (2004). Corticotrophin releasing factor-induced synaptic plasticity in the amygdala translates stress into emotional disorders. J. Neurosci. 24, 3471-3479.

Roozendaal, B., McEwen, B.S. and Chattarji, S. (2009). Stress, memory and the amygdala. *Nat. Rev. Neurosci.* **10**, 423-433.

bioRxiv preprint doi: https://doi.org/10.1101/777979; this version posted November 7, 2019. The copyright holder for this preprint (which was not certified by peer review) is the author/funder. All rights reserved. No reuse allowed without permission.

Sajdyk, T.J., Johnson PL, Leitermann RJ, Fitz SD, Dietrich A, Morin M, Gehlert DR, Urban JH, and Shekhar A. (2008). Neuropeptide Y in the amygdala induces long-term resilience to stress-induced reductions in social responses but not hypothalamic-adrenal-pituitary axis activity or hyperthermia. J. Neurosci. 28, 893-903 (2008).

Sajdyk, T.J., Schober, D.A. and Gehlert, D.R. (2002a). Neuropeptide Y receptor subtypes in the basolateral nucleus of the amygdala modulate anxiogenic responses in rats. Neuropharmacology 43, 1165-1172.

Sajdyk, T.J., Schober, D.A., Smiley, D.L. and Gehlert, D.R. (2002b). Neuropeptide Y-Y2 receptors mediate anxiety in the amygdala. Pharmacol. Biochem. Behav. 71, 419-423.

Sajdyk, T.J., Shekhar, A. and Gehlert, D.R. (2004). Interactions between NPY and CRF in the amygdala to regulate emotionality. Neuropeptides 38, 225-234.

Schmeltzer SN, Herman JP, **Sah R**. (2016) Neuropeptide Y (NPY) and posttraumatic stress disorder (PTSD): A translational update. Exp Neurol. 284:196-210.

Selcher, J.C., Xu, W., Hanson, J.E., Malenka, R.C. and Madison, D.V. (2012). Glutamate receptor subunit GluA1 is necessary for long-term potentiation and synapse unsilencing, but not long-term depression in mouse hippocampus. Brain Res. 1435: 8-14.

bioRxiv preprint doi: https://doi.org/10.1101/777979; this version posted November 7, 2019. The copyright holder for this preprint (which was not certified by peer review) is the author/funder. All rights reserved. No reuse allowed without permission.

Sholl, D.A. (1953). Dendritic organization in the neurons of the visual and motor cortices of the cat. J. Anat. 87, 387-406.

Silveira Villarroel, H., Bompolaki M, Mackay JP, Miranda Tapia AP, Michaelson SD, Leitermann RJ, Marr RA, Urban JH and Colmers WF. (2018). NPY Induces Stress Resilience via Downregulation of Ih in Principal Neurons of Rat Basolateral Amygdala. J. Neurosci. 38: 4505-4520.

Soll, R.M., Dinger, M.C., Lundell, I., Larhammer, D. and Beck-Sickinger, A.G. (2001). Novel analogues of neuropeptide Y with a preference for the Y1-receptor. Eur. J. Biochem. 268: 2828-2837.

Stanić D, Mulder J, Watanabe M, Hökfelt T. (2011). Characterization of NPY Y2 receptor protein expression in the mouse brain. II. Coexistence with NPY, the Y1 receptor, and other neurotransmitter-related molecules. J Comp Neurol. 519:1219-1257.

Stoppini, L., Buchs, P.A. and Muller, D. (1991). A simple method for organotypic cultures of nervous tissue. J. Neurosci. Methods 37, 173-182.

Taylor, A.L. (2012). What we talk about when we talk about capacitance measured with the voltage-clamp step method. J. Comput. Neurosci. 32, 167-175.

Vyas, A., Jadhav, S. and Chattarji, S. (2006). Prolonged behavioral stress enhances synaptic connectivity in the basolateral amygdala. Neuroscience 143, 387-393.

bioRxiv preprint doi: https://doi.org/10.1101/777979; this version posted November 7, 2019. The copyright holder for this preprint (which was not certified by peer review) is the author/funder. All rights reserved. No reuse allowed without permission.

Vyas, A., Mitra, R., Shankaranarayana Rao, B.S. and Chattarji, S. (2002). Chronic stress induces contrasting patterns of dendritic remodeling in hippocampal and amygdaloid neurons. J. Neurosci. 22, 6810-6818.

Vyas, A., Pillai, A.G. and Chattarji, S. (2004). Recovery after chronic stress fails to reverse amygdaloid neuronal hypertrophy and enhanced anxiety-like behavior. Neuroscience 128, 667-673.

Wahlestedt C, Yanaihara N and Håkanson R. (1986). Evidence for different pre-and post-junctional receptors for neuropeptide Y and related peptides. Regul Pept. 13:307-318.

Yehuda R, Brand S, Yang RK. (2006). Plasma neuropeptide Y concentrations in combat exposed veterans: relationship to trauma exposure, recovery from PTSD, and coping. Biol Psychiatry. 59:660-663.

Zhou Z, Zhu G, Hariri AR, Enoch MA, Scott D, Sinha R, Virkkunen M, Mash DC, Lipsky RH, Hu XZ, Hodgkinson CA, Xu K, Buzas B, Yuan Q, Shen PH, Ferrell RE, Manuck SB, Brown SM, Hauger RL, Stohler CS, Zubieta JK, Goldman D. (2008) Genetic variation in human NPY expression affects stress response and emotion. Nature 452:997-1001

bioRxiv preprint doi: https://doi.org/10.1101/777979; this version posted November 7, 2019. The copyright holder for this preprint (which was not certified by peer review) is the author/funder. All rights reserved. No reuse allowed without permission.

FIGURE LEGENDS

Figure 1. Experimental timelines and changes in principal neuron synaptic properties with repeated NPY or CRF treatment in BLA OTCs. a. Comparative timelines for experiments with BLA OTCs (upper timeline) and *in vivo* (lower timeline) models. **b,c** Representative electrophysiological recordings of spontaneous synaptic currents in BLA OTC principal neurons treated repeatedly with vehicle (**b)** and (**c**) 100 nM NPY, **d**. Mean sIPSC amplitudes in neurons in vehicle control (n=25) or 100 nM NPY (n=25) (Mann-Whitney U test; U = 171.0, p = 0.0054). **e**. Scatter plots of mean sEPSC interevent interval from recordings of cells in **c.** Vehicle control (n=25) or 100 nM NPY (n=25) (Mann-Whitney U test; U = 155.5, p = 0.0019) **f – g** Representative electrophysiological recordings of neurons treated repeatedly with vehicle or with 30 nM CRF. **h**. Mean sEPSC interevent interval in vehicle control (n=25) or 100 nM 30 nM CRF (n=25). (Mann-Whitney U test; U = 194, p = 0.0208). For **d, e, h**, circles represent neuron means, black bars represent population means and for all, error bars indicate s.e.m. All statistical tests were two-sided. **P<0.01.

Figure 2. NPY treatment of BLA OTC causes pyramidal neuron hypotrophy. a. Scatter plot of mean capacitance of OTC pyramidal neurons treated with vehicle ("Control" n=42), NPY at 100 pM (n=31), 1 nM (n=43), 10 nM (n=47), 100 nM (n=49) and the inactive analogue, desamido-NPY at 100 nM ("da" n=30) ($H_{(5)}$ = 40.72, p =1.07e^{-7}). ***Inset*** Representative capacitative transients for control- or 100 nM NPY-treated BLA OTC neurons. **b**. Scatter plot of mean total dendritic length for OTC neurons treated as in **a**. Vehicle (n=26), NPY at 100 pM (n=26), 1 nM (n=25), 10 nM (n=21), 100 nM (n=24) and da-NPY 100 nM (n=20) ($H_{(5)}$ = 19.04, p = 0.0019). **c.** Scatter plot of mean number of branch points in neurons in **b** ($H_{(5)}$ = 17.02, p = 0.0045). **d**. Sholl analysis of neurons in **b** and **c**

bioRxiv preprint doi: https://doi.org/10.1101/777979; this version posted November 7, 2019. The copyright holder for this preprint (which was not certified by peer review) is the author/funder. All rights reserved. No reuse allowed without permission.

treated as indicated (Treatment: $F_{(2, 72)} = 9.96$, $p = 0.00015$; Distance: $F_{(40, 2880)} = 185.4$, $p \sim 0$; Interaction: $F_{(80, 2880)} = 2.09$, $p = 8.57e^{-8}$). **e-j.** Representative reconstructions of neurons treated as indicated above. N-values for **c** and **d** are as in **b**. For **a-c**, Kruskal-Wallis H tests with Dunn's post hoc tests. For **d**, 2-way RM ANOVA with Tukey's post-hoc test. For **a-c**, circles represent neurons, black bars represent population means, while in **d**, symbols represent population means and for all, error bars indicate s.e.m. All tests were two-sided. **P*<0.05, ***P*<0.01, ****P*<0.001, *****P*<0.0001 for post hoc multiple comparisons. Scale bars in e-j = 100 µm.

Figure 3. Treatment with NPY, CRF or the Y_5R agonist, cPP, affects the estimated total number of spines per cell, but not spine density of principal neurons in BLA OTCs. a – c.. Representative images of spines on pyramidal neurons treated with vehicle control, 100 nM NPY, 100 nM cPP and 30 nM CRF, as indicated. **d**. Scatter plot of mean spine density of pyramidal neurons treated as in **a**. vehicle control (n=15), 100 nM NPY (n=15), 100 nM cPP (n=15) and 30 nM CRF (n=15); 1-way ANOVA with Dunnett's multiple comparisons test: $F_{(3, 56)} = 1.437$, $p = 0.24$. **e**. Scatter plot of mean estimated total number of spines for neurons in **d** (One-way ANOVA with Welch's correction and Dunnett's T3 multiple comparisons test $W_{(3, 29.15)} = 10.61$, $p = 7.09e^{-5}$). For **d,e,** circles represent neuron means, black bars represent population means and for all, error bars indicate s.e.m. All tests were two-sided. *P<0.05, **P<0.01, ***P<0.001, ****P<0.0001.

Figure 4. CRF treatment of BLA OTC causes pyramidal neuron hypertrophy. a. Scatter plot of mean capacitance of OTC pyramidal neurons treated with vehicle control (n=39) and CRF at 300 pM (n=40), 3 nM (n=36) and 30 nM (n=38) ($H_{(3)} = 22.67$, $p = 4.72e^{-5}$). ***Inset***. Representative capacitance transients from control- or 30 nM CRF-treated BLA OTC neurons. **b.** Scatter plot of

bioRxiv preprint doi: https://doi.org/10.1101/777979; this version posted November 7, 2019. The copyright holder for this preprint (which was not certified by peer review) is the author/funder. All rights reserved. No reuse allowed without permission.

mean total dendritic length for OTC neurons treated as in **a**. Vehicle control (n=33) and CRF at 300 pM (n=31), 3 nM (n=26) and 30 nM (n=28) ($H_{(3)}$ = 22.71, p =4.63e^{-5}). **c**. Scatter plot of mean number of branch points in neurons in **b** ($H_{(3)}$ = 19.90, p = 0.0002). **d**. Sholl analysis of neurons in **b** and **c** treated as indicated (Treatment: $F_{(2, 84)}$ = 11.43, p = 4.05e^{-5}; Distance: $F_{(40, 3360)}$ = 137.4, p ~ 0; Interaction: $F_{(80, 3360)}$ = 2.58, p = 1.45e^{-12}). **e**-**g**. Representative reconstructions of neurons treated as indicated above. For **a-c**, Kruskal-Wallis H tests with Dunn's post hoc tests. For **d**, 2-way RM ANOVA with Tukey's post-hoc test. For **a-c**, circles represent neurons, black bars represent population means, while in **d**, symbols represent population means and for all, error bars indicate s.e.m. All tests were two-sided. *P<0.05, **P<0.01, ***P<0.001, ****P<0.0001 for post hoc multiple comparisons. Scale bars in e-g = 100 µm.

Figure 5. Sequential treatment with either NPY or CRF reverses or prevents the effects of the other neuropeptide alone on BLA OTC pyramidal neuron morphology. **a**. Scatter plot of mean capacitance of OTC pyramidal neurons treated with media control (n=42), 30 nM CRF followed by 100 nM NPY (n=31) and 100 nM NPY followed by 30 nM CRF (n=32), with the mean capacitance for 30 nM CRF and 100 nM NPY alone (data from figs 1 and 2) indicated by dashed lines ($H_{(2)}$ = 0.73, p = 0.69). ***Inset*** Representative capacitance transients from control, CRF, NPY- and NPY, CRF-treated BLA OTC neurons. **b**. Scatter plot of mean total dendritic length for OTC neurons treated as in **a**. with control (n=26), CRF and NPY (n=23) and NPY and CRF (n=23) with the mean total length for 30 nM CRF and 100 nM NPY alone from Figs 1 and 2 as dashed lines ($H_{(2)}$ = 0.80, p = 0.67). **c**. Scatter plot of mean number of branch points in neurons in **b** with the mean values for 30 nM CRF and 100 nM NPY alone from Figs 1 and 2 as dashed lines ($H_{(2)}$ = 0.36, p = 0.84). **d**. Sholl analysis of neurons in **b** and **c** with the Sholl analysis for 30 nM CRF and 100 nM NPY from Figs 1

bioRxiv preprint doi: https://doi.org/10.1101/777979; this version posted November 7, 2019. The copyright holder for this preprint (which was not certified by peer review) is the author/funder. All rights reserved. No reuse allowed without permission.

and 2 as dashed lines (Treatment: $F_{(2, 69)} = 0.21$, $p = 0.81$; Distance: $F_{(40, 2760)} = 157.3$, $p \sim 0$; Interaction: $F_{(80, 2760)} = 0.70$, $p = 0.98$). **e-g**. Representative traces from neurons treated as indicated.. **h.** Mean sEPSC interevent interval in neurons treated with 30 nM CRF followed by 100 nM NPY (n=25), 100 nM NPY followed by 30 nM CRF (n=25), 30 nM CRF alone (n=25) and 100 nM NPY alone (n=25) ($H_{(3)} = 28.18$, $p = 3.33e^{-6}$). **i-k** representative recordings from neurons treated as indicated. Statistical tests: For **a-c**, Kruskal-Wallis H tests with Dunn's post hoc tests. For **d**, 2-way RM ANOVA with Tukey's post-hoc tests. For **h**, Kruskal-Wallis H test with Dunn's post hoc test. For **a-c**, circles represent individual neurons, black bars represent population means, while in **d**, symbols represent population means and for all, error bars indicate s.e.m. All statistical tests were two-sided. *P<0.05, **P<0.01, ***P<0.001, ****P<0.0001. Scale bars in e-j = 100 µm.

Figure 6. Treatment with the selective Y_1 receptor agonist F^7P^{34}-NPY does not affect BLA OTC pyramidal neuron morphology. a. Scatter plot of mean capacitance of OTC pyramidal neurons treated with vehicle control (n=30) and F^7P^{34}-NPY at 1 nM (n=28), 10 nM (n=34) and 100 nM (n=34) ($H_{(3)} = 0.58$, $p = 0.90$). ***Inset*** Representative capacitance transients from Control- and F^7P^{34} NPY-treated BLA OTC neurons. **b**. Scatter plot of mean total dendritic length for neurons treated as in **a**. vehicle control (n=27) and F^7P^{34}-NPY at 1 nM (n=19), 10 nM (n=18) and 100 nM (n=22) ($H_{(3)} = 1.04$, $p = 0.79$). **c**. Scatter plot of mean number of branch points for neurons in **b** ($H_{(3)} = 4.25$, $p = 0.24$). **d**. Sholl analysis for neurons in **b** and **c** treated as indicated (Treatment: $F_{(1, 48)} = 1.82$, $p = 0.18$; Distance: $F_{(40, 1920)} = 109.3$, $p \sim 0$; Interaction: $F_{(40, 1920)} = 0.33$, $p = 0.99$). For **a-c**, Kruskal-Wallis H tests with Dunn's post hoc tests. For **d**, 2-way RM ANOVA with Tukey's post-hoc test. For **a-c**, circles represent neurons, black bars represent population means, while in **d**, symbols represent population means and for all, error bars indicate s.e.m. All tests were two-sided.

bioRxiv preprint doi: https://doi.org/10.1101/777979; this version posted November 7, 2019. The copyright holder for this preprint (which was not certified by peer review) is the author/funder. All rights reserved. No reuse allowed without permission.

Figure 7. Treatment with the Y_1R agonist F^7P^{34}-NPY does not affect the sEPSC frequency, while the Y_5R agonist cPP reduces sEPSC frequency onto BLA OTC pyramidal neurons. **a-b,d-e**. Representative electrophysiological recordings of spontaneous synaptic currents in BLA OTC pyramidal neurons treated with (**a,d**) vehicle, (**b**) F^7P^{34}- NPYand (**e**) cPP. **c.** Scatter plot of mean interevent sEPSC intervals onto pyramidal neurons treated with vehicle (n=25) and 100 nM F^7P^{34}-NPY (n=25) (Mann-Whitney U test; U = 299.0, p = 0.80). **f.** Scatter plot of mean inter-event interval of sIPSC (t-test with Welch's correction: $t_{(36.20)}$ = 2.92, p = 0.0060) and sEPSCs (Mann-Whitney U test; U = 111.0, p <0.0001) from vehicle control (n=25) and cPP-treated neurons (n=25). **g.** Scatter plot of mean amplitudes of sIPSC (Mann-Whitney U test; U = 259.0, p =0.30) and sEPSCs (Mann-Whitney U test; U = 269.0, p =0.40) from vehicle control (n=25) and cPP (100 nM)-treated (n=25) neurons. For **c,f-g**, circles represent neuron means, black bars represent population means and for all, error bars indicate s.e.m. All statistical tests were two-sided. ns = P>0.05,*P<0.05, **P<0.01, ***P<0.001, ****P<0.0001.

Figure 8. Treatment of BLA OTCs with the Y_2R agonist ahx causes pyramidal neuron hypertrophy. **a**. Scatter plot of mean capacitance of OTC pyramidal neurons treated with vehicle (n=26), ahx at 1 nM (n=23), 10 nM (n=21), and 100 nM (n=25) ($H_{(3)}$ = 11.31, p = 0.010). **b**. Scatter plot of mean total dendritic length for OTC neurons treated as in **a** ($H_{(3)}$ = 13.25, p = 0.0041). Vehicle (n=23), ahx at 1 nM (n=19), 10 nM (n=23), and 100 nM (n=23). **c.** Scatter plot of mean number of branch points in neurons in **b** ($H_{(3)}$ = 17.94, p = 0.0005). **d**. Sholl analysis of neurons in **b** and **c** treated as indicated (<u>Treatment:</u> $F_{(2, 66)}$ = 4.06, p = 0.022; <u>Distance:</u> $F_{(40, 2640)}$ = 119.5, p ~ 0; <u>Interaction:</u> $F_{(80, 2640)}$ = 2.27,

bioRxiv preprint doi: https://doi.org/10.1101/777979; this version posted November 7, 2019. The copyright holder for this preprint (which was not certified by peer review) is the author/funder. All rights reserved. No reuse allowed without permission.

p = 1.92e^{-9}; Purple = control vs 10 nM ahx; Black = control vs 100 nM ahx). **e-g.** Representative reconstructions of neurons treated as indicated above. N-values for **c** and **d** are as in **b**. For **a-c**, Kruskal-Wallis H tests with Dunn's post hoc tests. For **d**, 2-way RM ANOVA with Tukey's post-hoc test. For **a-c**, circles represent neurons, black bars represent population means, while in **d**, symbols represent population means and for all, error bars indicate s.e.m. All tests were two-sided. **P*<0.05, ***P*<0.01, ****P*<0.001, *****P*<0.0001 for post hoc multiple comparisons. Scale bars in e-g = 100 µm.

Figure 9. Treatment of BLA OTC with the Y_5R agonist cPP results in pyramidal neuron hypotrophy, which is blocked by the Y_5R antagonist CGP71683A (Y_5A). **a**. Scatter plot of mean capacitance of OTC pyramidal neurons treated with vehicle control (n=30), cPP at 1 nM (n=32), 10 nM (n=47) and 100 nM and 10 nM NPY with 30 nM CGP (n=45) ($H_{(4)}$ = 33.61, p = 8.97e^{-7}). ***Inset*** Representative capacitance transients from Control-, cPP- and NPY + Y_5Antagonist-treated BLA OTC neurons. **b**. Scatter plot of mean total dendritic length of neurons treated as in **a**. vehicle control (n=26), cPP at 1 nM (n=23), 10 nM (n=31) and 100 nM (n=32) and 10 nM NPY with 30 nM CGP (n=34) ($H_{(4)}$ = 49.88, p = 3.83e^{-10}). **c**. Mean number of branch points in neurons in **b** ($H_{(4)}$ = 36.99, p = 1.81e^{-7}). **d.** Sholl analysis for neurons in **b** and **c** treated as indicated (<u>Treatment:</u> $F_{(2, 90)}$ = 23.98, p = 4.49e^{-9}; <u>Distance:</u> $F_{(40, 3600)}$ = 175.1, p ~ 0; <u>Interaction:</u> $F_{(80, 3600)}$ = 3.91, p <u>= 2.68e^{-28}</u>). Black = control vs. 100 nM cPP; Green = control vs. NPY + Y_5A; Blue = 100 nM cPP vs. NPY + Y_5A. **e-g**. Representative traces from neurons treated as indicated. For **a-c**, Kruskal-Wallis H tests with Dunn's post hoc tests. For **d**, 2-way RM ANOVA with Tukey's post-hoc test. For **a-c**, circles represent neurons, black bars represent population means, while in **d**, symbols represent population means and for all, error bars indicate s.e.m. All tests were two-sided. **P*<0.05,

bioRxiv preprint doi: https://doi.org/10.1101/777979; this version posted November 7, 2019. The copyright holder for this preprint (which was not certified by peer review) is the author/funder. All rights reserved. No reuse allowed without permission.

**P<0.01, ***P<0.001, ****P<0.0001 for post hoc multiple comparisons. Scale bars in e-g = 100 µm.

Figure 10. Repeated *in vivo* injection of NPY or the Y_5 receptor agonist, but not the Y_1 receptor agonist results in increased social interaction times and dendritic hypotrophy. **a**. Scatter plot depicting social interaction time shown as percent of individual animals' baselines for treatment with vehicle control (100 nL) at day 1 (n=50), day 5 (n=49), week 2 (n=43) and week 4 (n=19); NPY (10 pmol/100 nL) at day 1 (n=42), day 5 (n=40), week 2 (n=29) and week 4 (n=11); the Y_1 agonist F^7P^{34}-NPY (10 pmol/100 nL) at day 1 (n=15), day 5 (n=14), week 2 (n=14) and week 4 (n=10); the Y_5 agonist cPP (10 pmol/100 nL) at day 1 (n=7), day 5 (n=7), week 2 (n=7) and week 4 (n=7); and NPY (10 pmol/100 nL) immediately preceded by the Y_5 receptor antagonist CGP71683A (Y_5A, 10 pmol/100 nL) at day 1 (n=5), day 5 (n=5), week 2 (n=5) and week 4 (n=5) (Linear Mixed-model; Treatment: $F_{(4, 102.30)} = 14.11$, $p = 3.33e^{-9}$; Time: $F_{(3, 93.88)} = 1.66$, $p = 0.18$; Treatment * Time: $F_{(12, 91.12)} = 1.87$, $p = 0.049$). **b**. Scatter plot of mean capacitance of BLA pyramidal neurons in acute slices treated with vehicle control (n=64), NPY (n=53), F^7P^{34}-NPY (n=57), cPP (n=57) and NPY with CGP (n=51) (Kruskal-Wallis H test with Dunn's post hoc test; $H_{(4)} = 47.74$, $p = 1.07e^{-9}$). ***Inset*** Representative capacitance transients from Vehicle, NPY, F^7P^{34}-NPY, cPP and NPY + Y_5Antagonist injected acute slices. **c**. Scatter plot of mean total dendritic length for cells treated as in **b** (ANOVA with Tukey's post hoc; $F_{(4, 205)} = 17.70$, $p = 1.70e^{-12}$). vehicle (n=52), NPY (n=38), F^7P^{34}-NPY (n=32), cPP (n=50) and NPY with CGP (n=39). **d**. Scatter plot of mean number of branch points for neurons in **c** (Kruskal-Wallis H test with Dunn's post hoc test; $H_{(4)} = 56.53$, $p = 1.55e^{-11}$). **e**. Sholl analysis for neurons in **c** and **d** as indicated (2-way RM ANOVA with Tukey's post hoc test; <u>Treatment:</u> $F_{(4, 181)} = 13.09$, $p = 2.18e^{-9}$; <u>Distance:</u> $F_{(49, 8869)} = 815.7$, $p = \sim 0$; <u>Interaction:</u> $F_{(196, 8869)} = 4.81$, $p = 1.23e^{-91}$).

bioRxiv preprint doi: https://doi.org/10.1101/777979; this version posted November 7, 2019. The copyright holder for this preprint (which was not certified by peer review) is the author/funder. All rights reserved. No reuse allowed without permission.

Blue = vehicle vs. NPY; Green = vehicle vs. cPP. **f**-**j**. Representative traces from neurons treated as indicated above. For **a**, symbols represent animals and black bars represent population means. For **b-d**, circles represent neurons and black bars represent population means. For **e**, symbols represent population means and for all, error bars indicate s.e.m. All tests were two-sided. **P*<0.05, ***P*<0.01, ****P*<0.001, *****P*<0.0001 for post hoc multiple comparisons. Scale bars in f-j = 100 µm.

Figure 11. Inhibitors of Calcineurin (CsA) and of CaMKII (AIP) respectively block NPY- and CRF-mediated dendritic remodeling in BLA OTCs. a. Scatter plot of mean capacitance of BLA OTC pyramidal neurons treated with vehicle control (n=28) compared to CsA (2 nM) alone (n=35), CsA (2 nM) + NPY (10 nM) (n=31), OA (10 nM) alone (n=39) and OA (10 nM) + cPP (10 nM) (n=38) ($H_{(4)}$ = 22.80, p = 0.0001). Dashed lines represent mean for neurons treated with NPY (10 nM) (blue) and cPP (100 nM) (green). **b**. Scatter plot of mean total dendritic length of pyramidal neurons treated as in **a**, vehicle (n=26), CsA (n=26), CsA + NPY (n=30), OA (n=26) and OA + cPP (n=24) ($H_{(4)}$ = 27.88, p = 1.32e^{-5}). **c.** Scatter plot of mean number of branch points for neurons in **b** and **c,** with dashed lines representing the mean for neurons treated with NPY (blue) or cPP (green) ($H_{(4)}$ = 28.93, p = 8.10e^{-6}). **d**. Sholl analysis for neurons in **b** treated as indicated, data for neurons treated with NPY (blue) or cPP (green). Black = control vs. OA + cPP; Gray = control vs. CsA + NPY (<u>Treatment:</u> $F_{(2, 78)}$ = 11.86, p = 3.18e^{-5}; <u>Distance:</u> $F_{(40, 3120)}$ = 150.0, p ~ 0.; <u>Interaction:</u> $F_{(80, 3120)}$ = 2.39, p = 1.15e^{-10}). **e**. Scatter plot of mean capacitance values for BLA OTC pyramidal cells treated with vehicle (n=28), AIP (40 nM) (n=27) and AIP (40 nM) + CRF (30 nM) (n=29), with dashed line

bioRxiv preprint doi: https://doi.org/10.1101/777979; this version posted November 7, 2019. The copyright holder for this preprint (which was not certified by peer review) is the author/funder. All rights reserved. No reuse allowed without permission.

representing neurons treated with CRF ($H_{(2)} = 0.77$, $p = 0.68$). **f**. Scatter plot of mean total dendritic length for pyramidal cells treated as in **e** with neurons treated with CRF (dashed line) ($H_{(2)} = 1.23$, $p = 0.54$). Vehicle (n=26), AIP (n=21) and AIP + CRF (n=21). **g**. Scatter plot of mean number of branch points in neurons in **f** with the mean for neurons treated with CRF (dashed line) ($H_{(2)} = 0.81$, $p = 0.67$). **h**. Sholl analysis for neurons in **f** and **g** treated as indicated compared with neurons treated with CRF (dashed line) (Treatment: $F_{(2, 65)} = 0.50$, $p = 0.61$; Distance: $F_{(40, 2600)} = 165.3$, $p \sim 0$; Interaction: $F_{(80, 2600)} = 0.48$, $p = 0.99$). For **a-c,e-g**, Kruskal-Wallis H tests with Dunn's post hoc tests. For **d,h**, 2-way RM ANOVA with Tukey's post-hoc tests. For **a-c,e-g**, circles represent neurons, black bars represent population means, while in **d,h**, symbols represent population means and for all, error bars indicate s.e.m. All tests were two-sided. *P<0.05, **P<0.01, ***P<0.001, ****P<0.0001 for post hoc multiple comparisons.

Figure 12. Proposed model for the mechanism of action of NPY and CRF leading to dendritic hypotrophy or hypertrophy respectively in BLA pyramidal cells. a. NPY treatment results in net activation of the Y_5R and PP2B (Calcineurin), resulting in a reduction in dendritic arborization (illustrated right). **b.** CRF treatment results in net activation of CaMKII and hypertrophy of the dendritic arbor. (Illustrated right).

Figure 13. Correlation between whole-cell capacitance and dendritic length. a. Whole-cell capacitance plotted against total dendritic length for 259 BLA OTC neurons from 100 different OTCs taken from all experimental groups.

bioRxiv preprint doi: https://doi.org/10.1101/777979; this version posted November 7, 2019. The copyright holder for this preprint (which was not certified by peer review) is the author/funder. All rights reserved. No reuse allowed without permission.

TABLES

	Acute P14	Acute 10W	OTC EP 10W	ANOVA
RMP (mV)	-76.8 ± 0.5 *** n=56	-81.3 ± 0.7 n=44	-77.9 ± 1.0** n=54	F(2, 151) = 9.05, p= 0.0002
Rheobase (pA)	126.3 ± 5.2 **** n=56	309.2 ± 13.8 n=44	248.2 ± 24.8*, #### n=54	F(2, 151) = 29.84, p = 0.00019
I_R (MΩ)	176.8 ± 6.4 **** n=56	71.5 ± 5.2 n=22	103.4 ± 6.3*, #### n=49	F(2, 124) = 64.16, p = 7.43e-20
I_h max (pA)	-175.2 ± 7.3*** n=52	-362.5 ± 25.9 n=48	-290.4 ± 20.1*, ### n=49	F(2, 146) = 25.09, P = 4.31e-10
I_h density (pA/pF)	-0.96 ± 0.03 * n=52	-1.36 ± 0.10 n=22	-1.64 ± 0.13 #### n=49	F(2, 120) = 14.38, p=2.52e-6
C_m (pF)	180.2 ± 3.7 **** N=56	230.6 ± 7.3 N=44	150.0 ± 5.8 ****, ### N=58	F(2, 155) = 49.98 P=1.75e-18,
sIPSC AMP (pA)	25.5 ± 1.1 n=25	24.13 ± 1.8 n=25	49.8 ± 4.9 ****, #### n=25	F(2, 72) = 21.59, p=4.51e-8
sIPSC IEI (ms)	2249 ± 417 **** n=25	213.9 ± 22.1 n=25	155.6 ± 19.3 #### n=25	F(2, 72) = 24.41 p= 8.07e-9
sEPSC AMP (pA)	25.9 ± 0.9 n=25	26.87 ± 2.3 n=25	44.8 ± 2.1 ****, #### n=25	F(2, 72) = 32.15 p = 1.05e-10
sEPSC IEI (ms)	1241 ± 347.2 ** n=25	171.1 ± 26.4 n=25	221.5 ± 32.2 ## n=25	F(2, 72) = 8.95 p=0.0003
Total Dendritic Length (µm)	5986 ± 337 **** n=17	8644 ± 284 n=36	3625 ± 187.4****, ####, n=39	F(2, 89) = 113.6 p = 3.16e-25
# of branches	37.5 ± 2.3 * n=17	46.3 ± 1.9 n=36	20.5 ± 1.5 ****, #### n=39	F(2, 89) = 60.17 p = 2.95e-17

Table 1. Comparison of electrophysiological and morphological properties of acute P14, acute 10W and EP 10W OTC pyramidal neurons in the BLA.

Data presented as mean ± s.e.m. One-way ANOVA with Tukey's post-hoc test for multiple comparisons were used for all analyses; *P<0.05, **P<0.01, ***P<0.001, ****P<0.0001 vs Acute 10W, #P<0.05, ##P<0.01, ###P<0.001, ####P<0.0001 vs Acute P14 for multiple comparisons.

bioRxiv preprint doi: https://doi.org/10.1101/777979; this version posted November 7, 2019. The copyright holder for this preprint (which was not certified by peer review) is the author/funder. All rights reserved. No reuse allowed without permission.

Electrophysiological Figures					Morphology Figures				
Figure	**Treatment**	**Neurons**	**Cultures**	**Animals**	**Figure**	**Treatment**	**Neurons**	**Cultures**	**Animals**
1c,d	Control	25	11	5	2b-d	Control	26	19	16
1c,d	NPY ($1e^{-7}$ M)	25	13	7	2b-d	NPY ($1e^{-10}$ M)	26	14	3
1g	Control	25	14	8	2b-d	NPY ($1e^{-9}$ M)	25	16	15
1g	CRF ($3e^{-8}$ M)	25	16	9	2b-d	NPY ($1e^{-8}$ M)	21	16	14
2a	Control	42	20	18	2b-d	NPY ($1e^{-7}$ M)	24	16	13
2a	NPY ($1e^{-10}$ M)	31	15	3	2b-d	da-NPY ($1e^{-7}$ M)	20	12	11
2a	NPY ($1e^{-9}$ M)	43	25	23	3d,e	Control	15	11	6
2a	NPY ($1e^{-8}$ M)	47	27	20	3d,e	NPY ($1e^{-7}$ M)	15	10	6
2a	NPY ($1e^{-7}$ M)	49	26	21	3d,e	CRF ($3e^{-8}$ M)	15	10	5
2a	da-NPY ($1e^{-7}$ M)	30	14	13	3d,e	cPP ($1e^{-7}$ M)	15	8	5
4a	Control	39	19	14	4b-d	Control	33	19	14
4a	CRF ($3e^{-10}$ M)	40	21	11	4b-d	CRF ($3e^{-10}$ M)	31	19	11
4a	CRF ($3e^{-9}$ M)	36	18	11	4b-d	CRF ($3e^{-9}$ M)	26	15	11
4a	CRF ($3e^{-8}$ M)	38	20	11	4b-d	CRF ($3e^{-8}$ M)	28	18	10
5a	Control	42	24	21	5b-d	Control	26	21	16
5a	CRF-NPY	31	15	6	5b-d	CRF-NPY	23	13	6
5a	NPY-CRF	32	15	7	5b-d	NPY-CRF	23	12	6
5h	CRF-NPY	25	12	5	6b-d	Control	27	15	13
5h	NPY-CRF	25	10	4	6b-d	F^7P^{34}-NPY ($1e^{-9}$ M)	19	14	12
6a	Control	30	22	19	6b-d	F^7P^{34}-NPY ($1e^{-8}$ M)	18	15	10
6a	F^7P^{34}-NPY (1^{e-9} M)	28	19	15	6b-d	F^7P^{34}-NPY ($1e^{-7}$ M)	22	14	13
6a	F^7P^{34}-NPY ($1e^{-8}$ M)	34	20	14	8b-d	Control	23	11	9
6a	F^7P^{34}-NPY ($1e^{-7}$ M)	34	22	18	8b-d	ahx ($1e^{-9}$ M)	19	11	10
7c	Control	25	15	9	8b-d	ahx ($1e^{-8}$ M)	23	15	13
7c	F^7P^{34}-NPY ($1e^{-7}$ M)	25	18	13	8b-d	ahx ($1e^{-7}$ M)	23	13	10
7f,g	Control	25	15	9	9b-d	Control	26	17	13
7f,g	cPP ($1e^{-7}$ M)	25	14	8	9b-d	cPP ($1e^{-9}$ M)	23	17	11
8a	Control	26	12	9	9b-d	cPP ($1e^{-8}$ M)	31	17	12
8a	ahx ($1e^{-9}$ M)	23	10	8	9b-d	cPP ($1e^{-7}$ M)	32	17	13
8a	ahx ($1e^{-8}$ M)	21	12	8	9b-d	NPY ($1e^{-8}$ M) + CGP (3^{e-8} M)	34	17	5
8a	ahx ($1e^{-7}$ M)	25	14	10	11b-d	Control	26	17	4
9a	Control	30	20	13	11b-d	CsA ($2e^{-9}$ M)	26	14	4
9a	cPP ($1e^{-9}$ M)	32	18	12	11b-d	CsA ($2e^{-9}$ M) + NPY ($1e^{-8}$ M)	30	17	4
9a	cPP ($1e^{-8}$ M)	47	26	16	11b-d	OA ($1e^{-8}$ M)	26	12	4
9a	cPP ($1e^{-7}$ M)	34	23	15	11b-d	OA ($1e^{-8}$ M) + cPP ($1e^{-7}$ M)	24	13	4
9a	NPY ($1e^{-8}$ M) + CGP ($3e^{-8}$ M)	45	25	6	11f-g	Control	26	13	10
11a	Control	28	17	4	11f-g	AIP ($4e^{-8}$ M)	21	10	4
11a	CsA ($2e^{-9}$ M)	35	16	4	11f-g	AIP ($4e^{-8}$ M) + CRF ($3e^{-8}$ M)	21	11	4
11a	CsA ($2e^{-9}$ M) + NPY ($1e^{-8}$ M)	31	18	4					
11a	OA ($1e^{-8}$ M)	39	15	4					

bioRxiv preprint doi: https://doi.org/10.1101/777979; this version posted November 7, 2019. The copyright holder for this preprint (which was not certified by peer review) is the author/funder. All rights reserved. No reuse allowed without permission.

11a	OA ($1e^{-8}$ M) + cPP ($1e^{-7}$ M)	38	15	4					
11e	Control	28	15	11					
11e	AIP ($4e^{-8}$ M)	27	13	4					
11e	AIP ($4e^{-8}$ M) + CRF ($3e^{-8}$ M)	29	14	4					

Table 2. Numbers of neurons, OTCs and animals used for capacitance and morphological analysis, indexed by Figure.

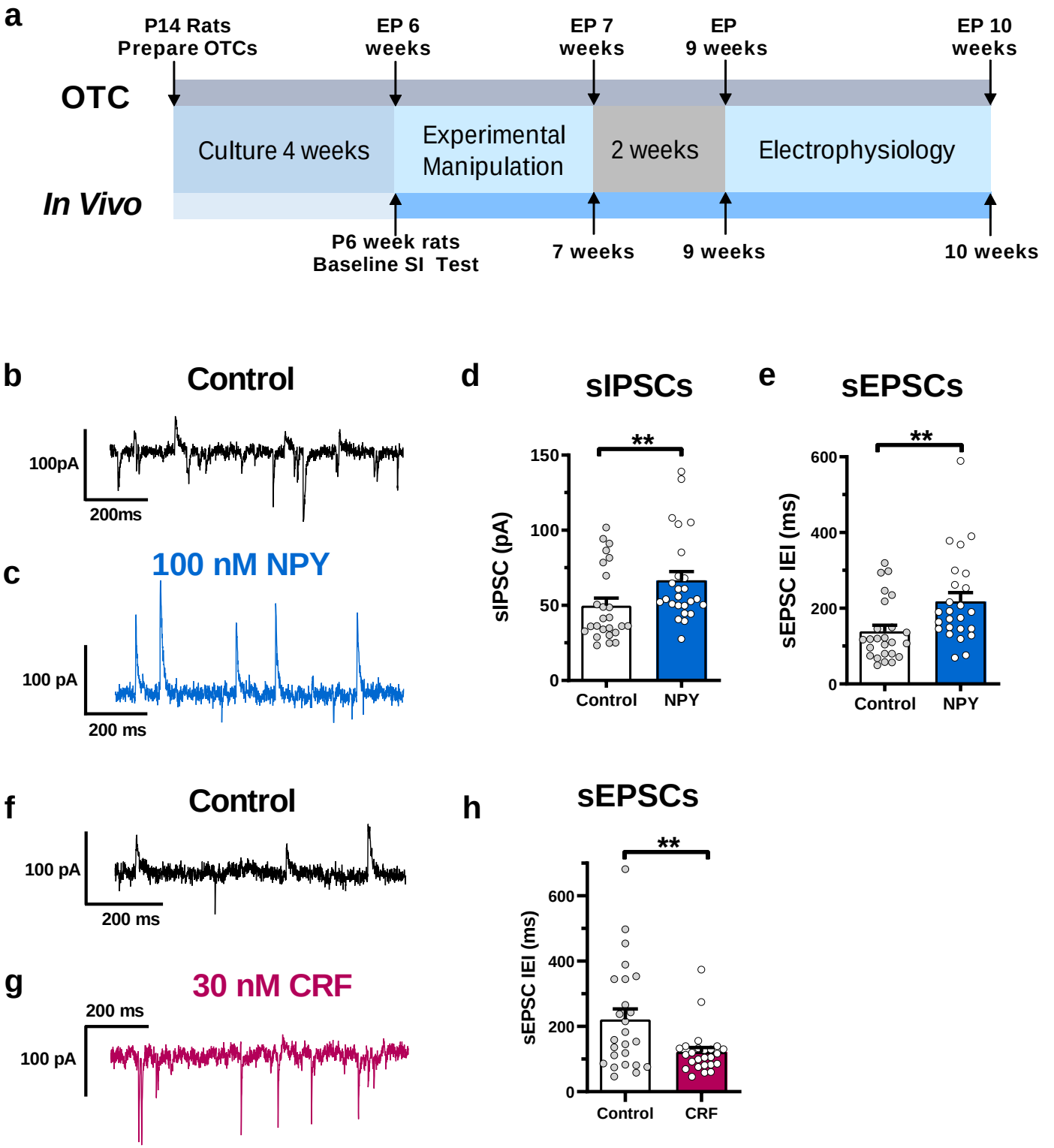
a
P14 Rats
Prepare OTCs
EP 6
weeks
EP 7
weeks
EP
9 weeks
EP 10
weeks
OTC
Culture 4 weeks
Experimental
Manipulation
2 weeks
Electrophysiology
In Vivo
P6 week rats
Baseline SI Test
7 weeks
9 weeks
10 weeks
b
Control
100pA
200ms
c
100 nM NPY
100 pA
200 ms
d
sIPSCs
sIPSC (pA)
150
100
50
0
**
Control
NPY
e
sEPSCs
sEPSC IEI (ms)
600
400
200
0
**
Control
NPY
f
Control
100 pA
200 ms
g
30 nM CRF
200 ms
100 pA
h
sEPSCs
sEPSC IEI (ms)
600
400
200
0
**
Control
CRF

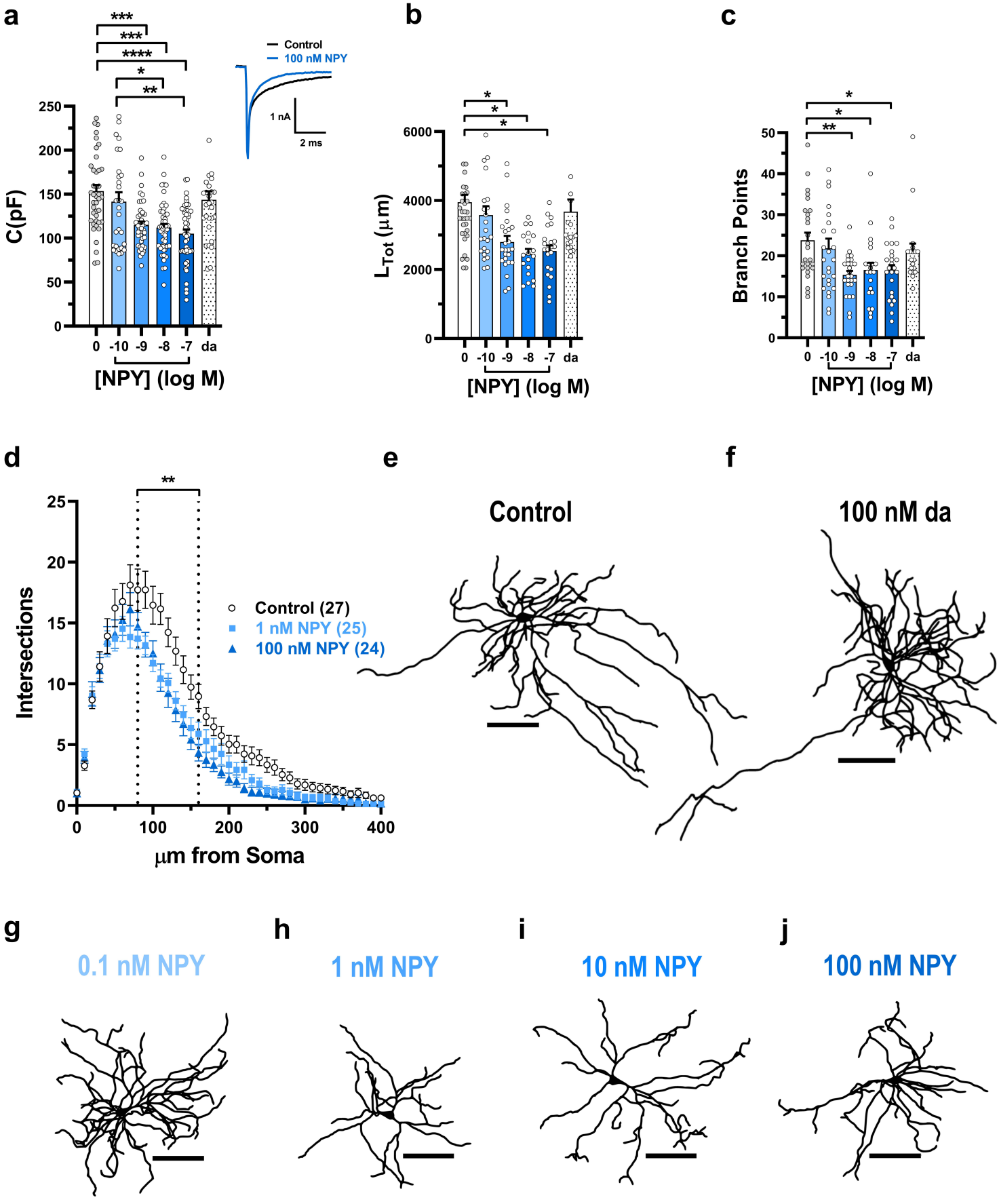
a
***
***
****
*
**
Control
100 nM NPY
1 nA
2 ms
C(pF)
250
200
150
100
50
0
0 -10 -9 -8 -7 da
[NPY] (log M)
b
*
*
*
L_{Tot} (µm)
6000
4000
2000
0
0 -10 -9 -8 -7 da
[NPY] (log M)
c
*
*
**
Branch Points
50
40
30
20
10
0
0 -10 -9 -8 -7 da
[NPY] (log M)
d
**
Intersections
25
20
15
10
5
0
0
100
200
300
400
µm from Soma
Control (27)
1 nM NPY (25)
100 nM NPY (24)
e
Control
f
100 nM da
g
0.1 nM NPY
h
1 nM NPY
i
10 nM NPY
j
100 nM NPY

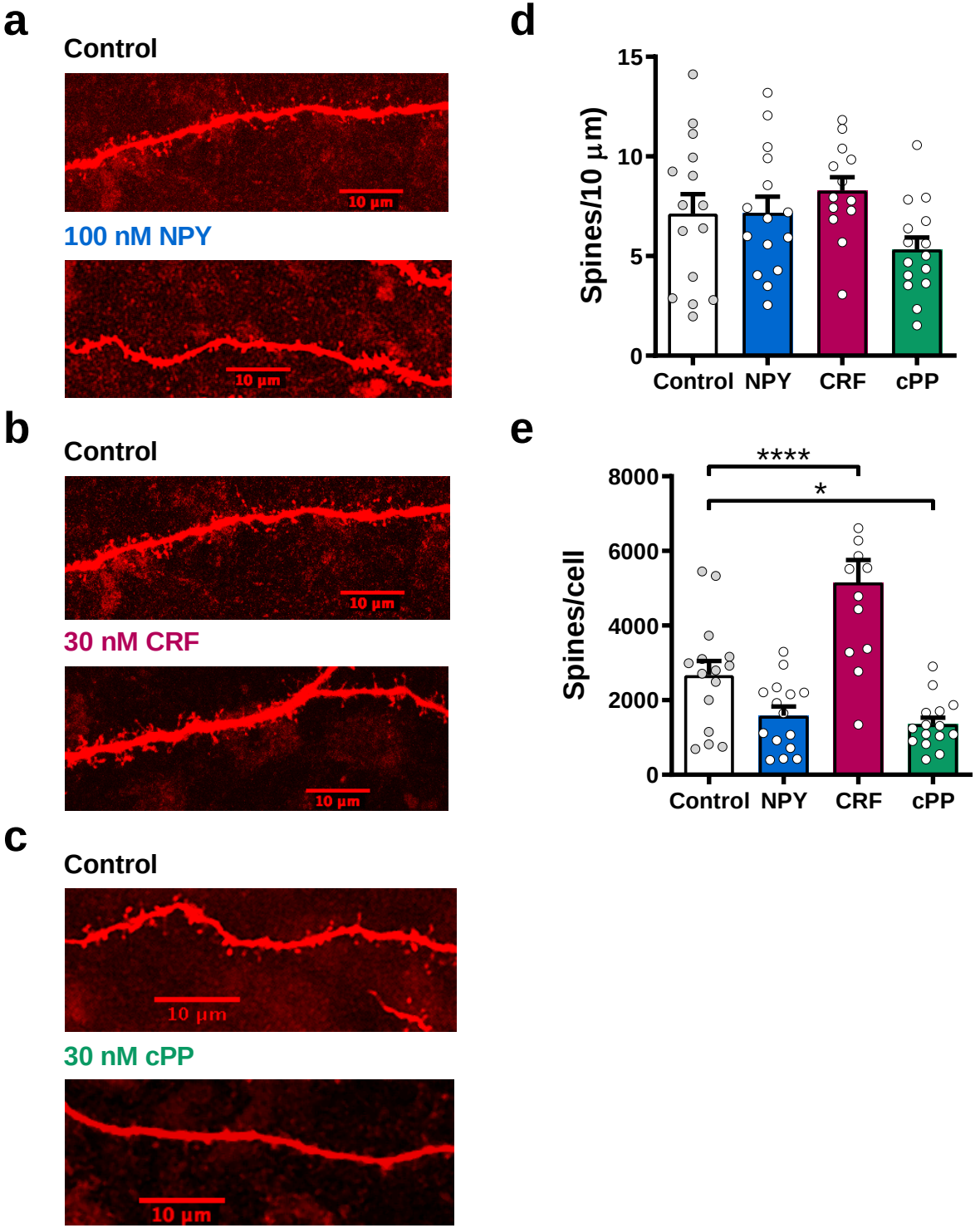
a
Control
10 µm
100 nM NPY
10 µm
b
Control
10 µm
30 nM CRF
10 µm
c
Control
10 µm
30 nM cPP
10 µm
d
Spines/10 µm)
15
10
5
0
Control
NPY
CRF
cPP
e
Spines/cell
8000
6000
4000
2000
0
****
*
Control
NPY
CRF
cPP

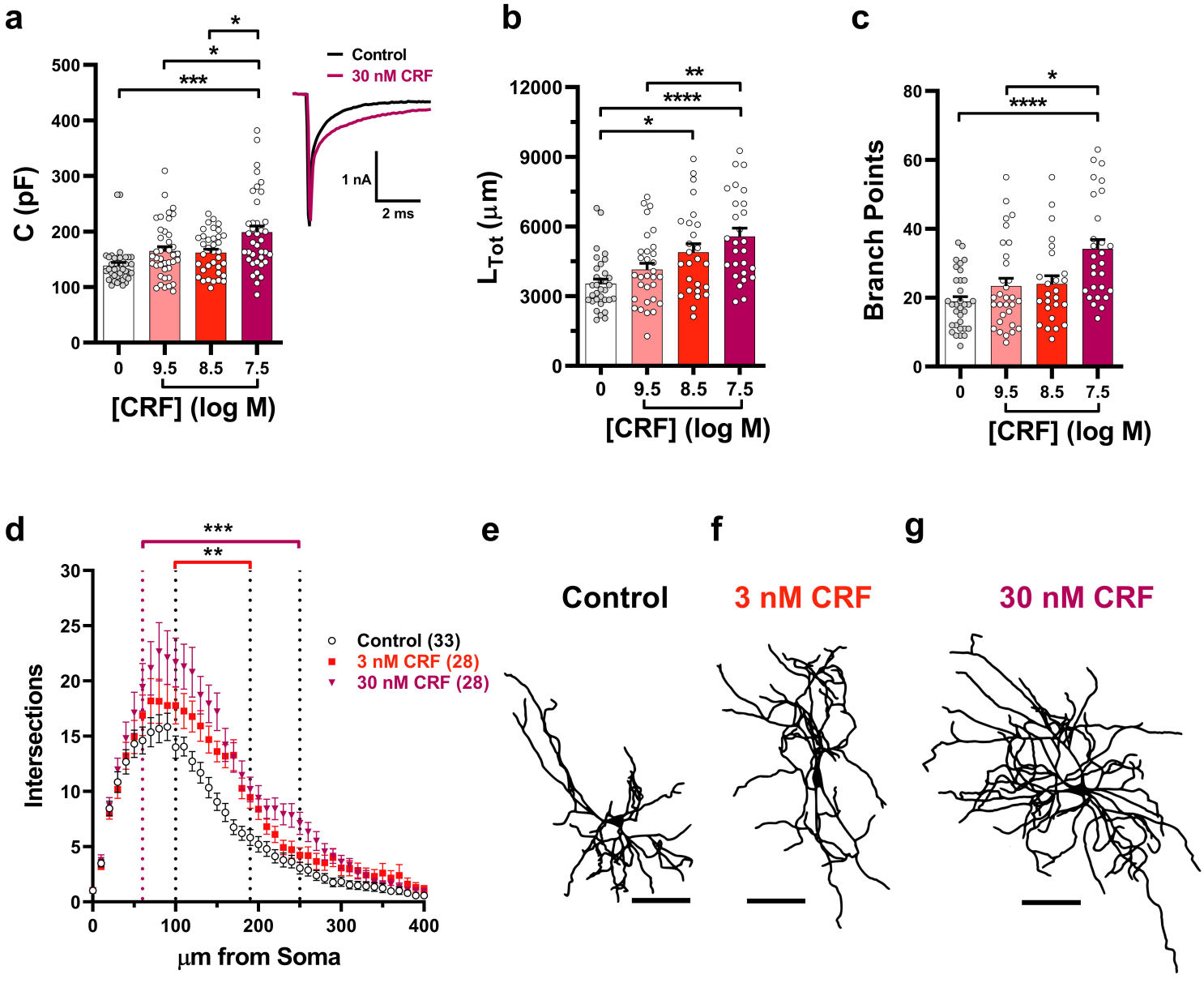
a
C (pF)
500
400
300
200
100
0
***
*
*
0
9.5
8.5
7.5
[CRF] (log M)
Control
30 nM CRF
1 nA
2 ms
b
L_{Tot} (µm)
12000
9000
6000
3000
0
**
****
*
0
9.5
8.5
7.5
[CRF] (log M)
c
Branch Points
80
60
40
20
0
*
****
0
9.5
8.5
7.5
[CRF] (log M)
d
Intersections
30
25
20
15
10
5
0
***
**
0
100
200
300
400
µm from Soma
Control (33)
3 nM CRF (28)
30 nM CRF (28)
e
Control
f
3 nM CRF
g
30 nM CRF

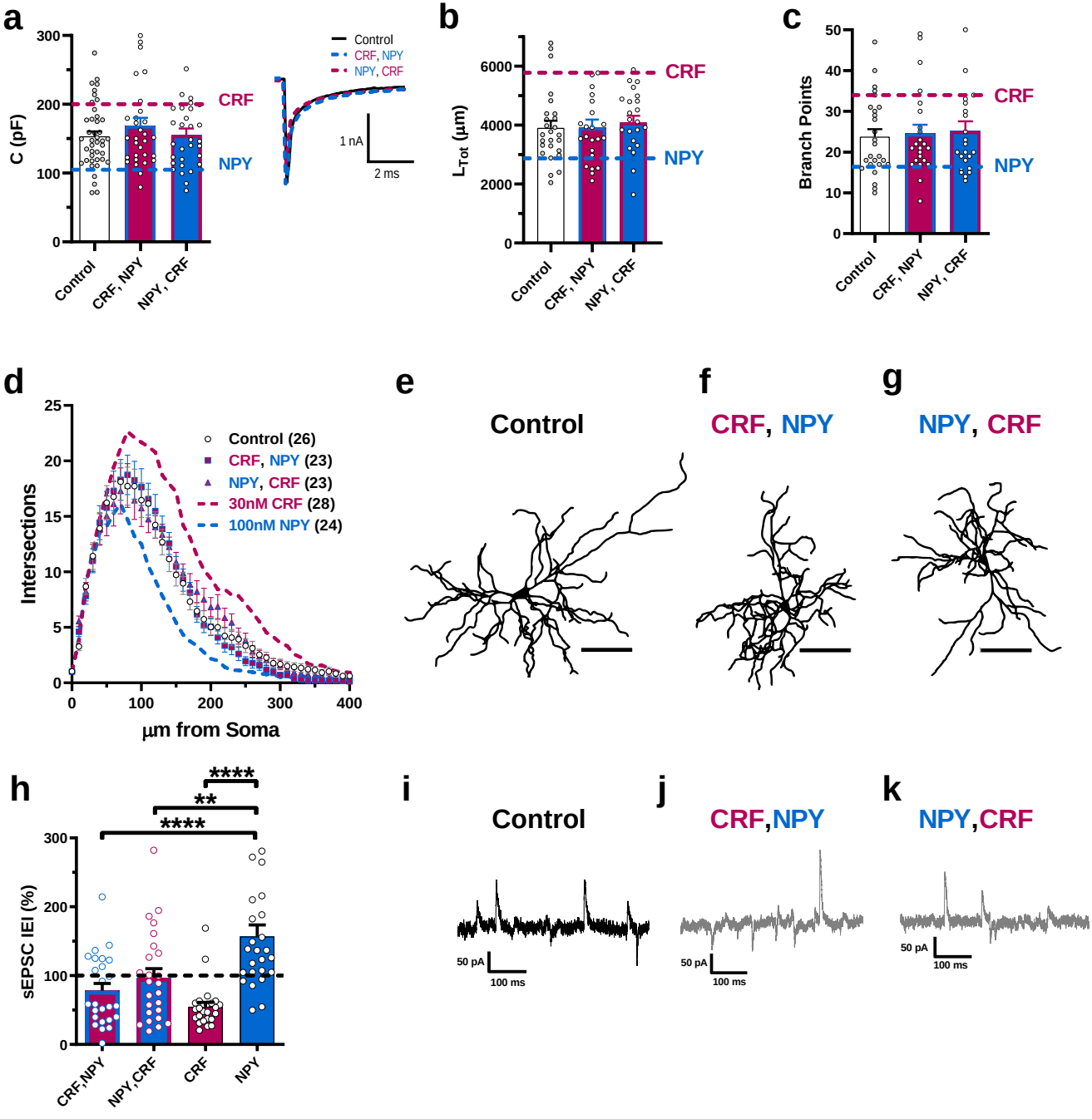
a
C (pF)
300
200
100
0
CRF
NPY
Control
CRF, NPY
NPY, CRF
Control
CRF, NPY
NPY, CRF
1 nA
2 ms
b
L_{Tot} (µm)
6000
4000
2000
0
CRF
NPY
Control
CRF, NPY
NPY, CRF
c
Branch Points
50
40
30
20
10
0
CRF
NPY
Control
CRF, NPY
NPY, CRF
d
Intersections
25
20
15
10
5
0
Control (26)
CRF, NPY (23)
NPY, CRF (23)
30nM CRF (28)
100nM NPY (24)
0
100
200
300
400
µm from Soma
e
Control
f
CRF, NPY
g
NPY, CRF
h
sEPSC IEI (%)
300
200
100
0
****
**
****
CRF,NPY
NPY,CRF
CRF
NPY
i
Control
50 pA
100 ms
j
CRF,NPY
50 pA
100 ms
k
NPY,CRF
50 pA
100 ms

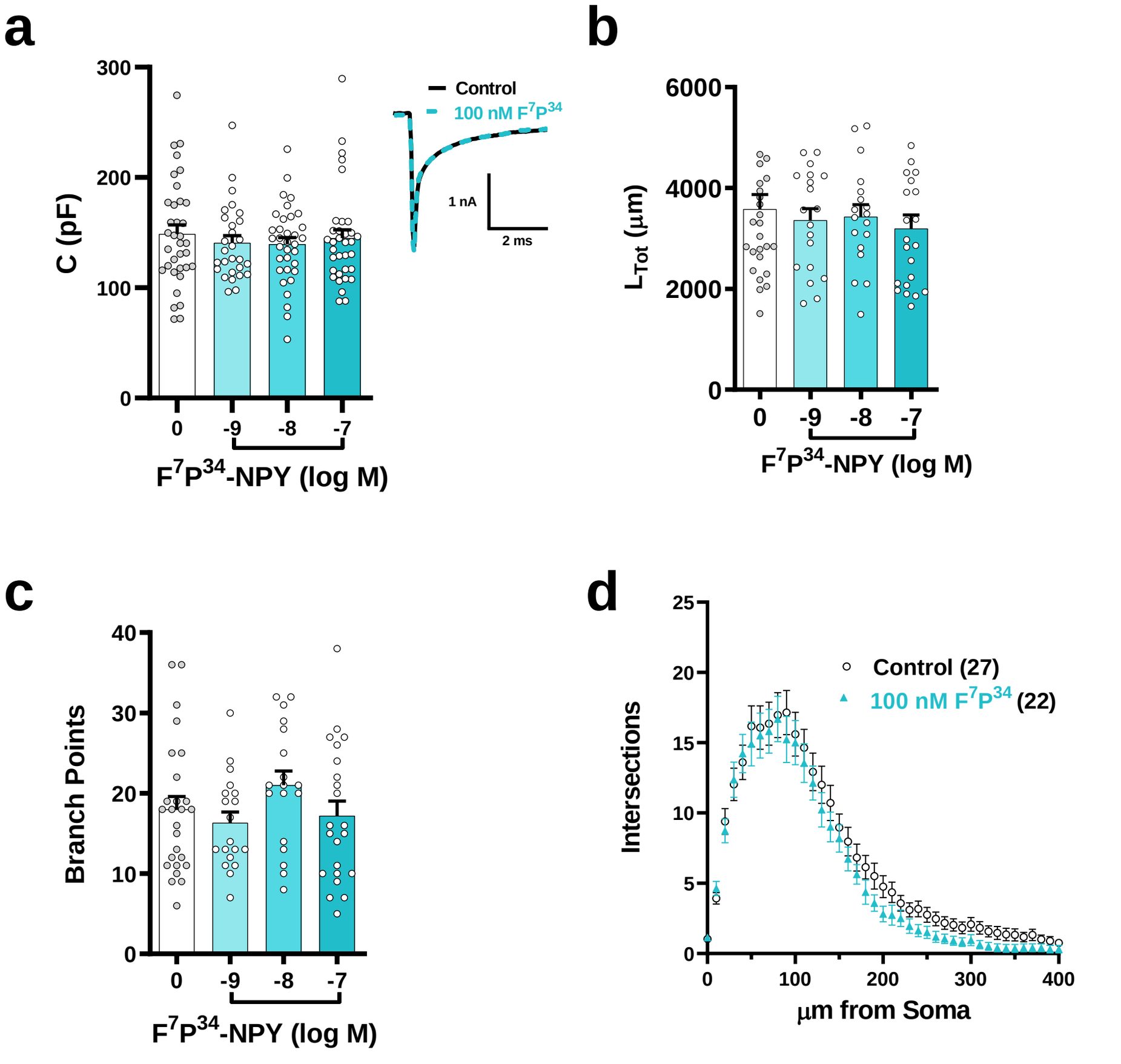
a
300
200
100
0
C (pF)
0
-9
-8
-7
F7P34-NPY (log M)
Control
100 nM F7P34
1 nA
2 ms
b
6000
4000
2000
0
LTot (µm)
0
-9
-8
-7
F7P34-NPY (log M)
c
40
30
20
10
0
Branch Points
0
-9
-8
-7
F7P34-NPY (log M)
d
25
20
15
10
5
0
Intersections
Control (27)
100 nM F7P34 (22)
0
100
200
300
400
µm from Soma

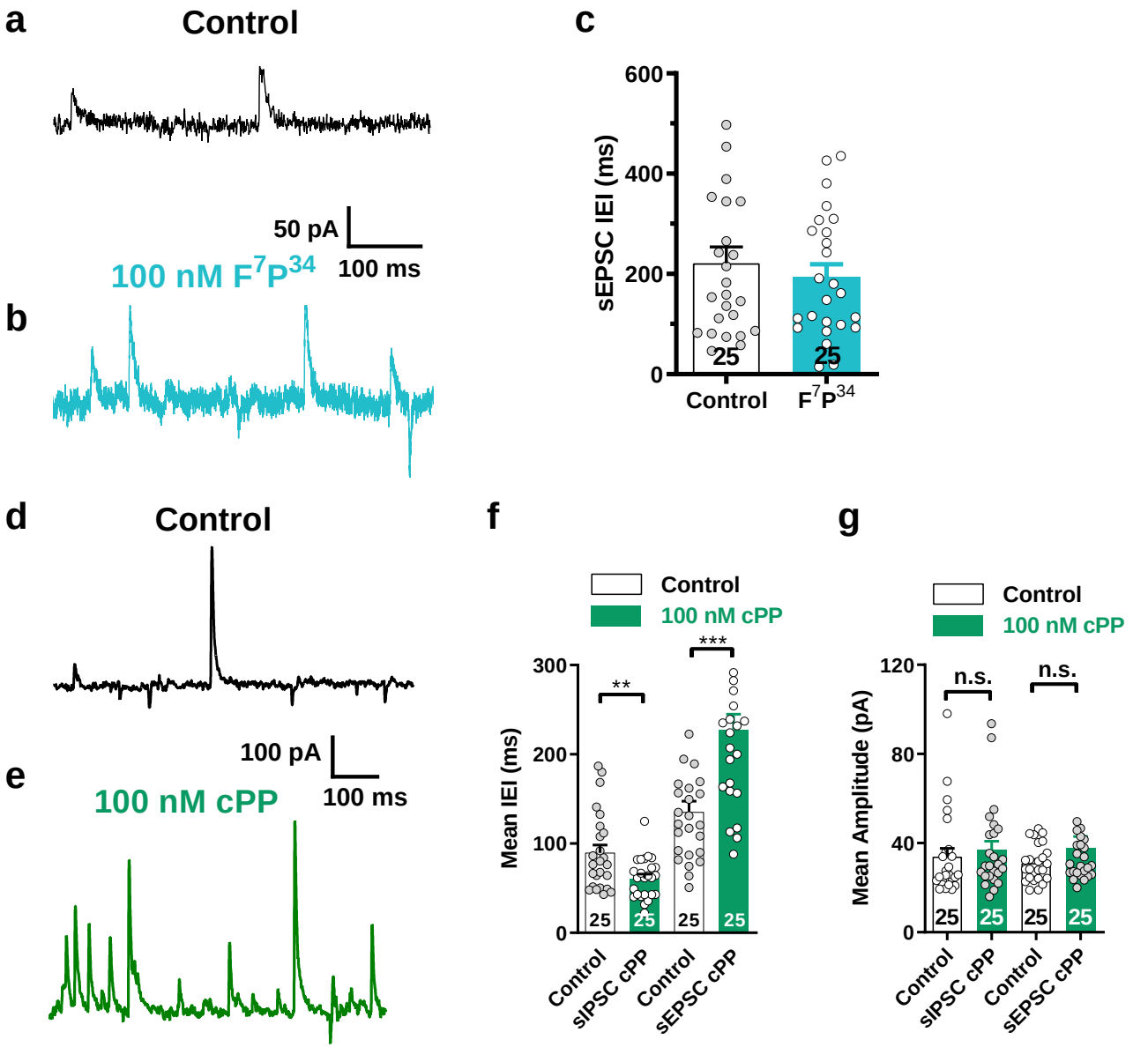
a
Control
50 pA
100 ms
100 nM F7P34
b
c
sEPSC IEI (ms)
600
400
200
0
25
25
Control
F7P34
d
Control
100 pA
100 ms
e
100 nM cPP
f
Control
100 nM cPP
Mean IEI (ms)
300
200
100
0
**
***
25
25
25
25
Control
sIPSC cPP
Control
sEPSC cPP
g
Control
100 nM cPP
Mean Amplitude (pA)
120
80
40
0
n.s.
n.s.
25
25
25
25
Control
sIPSC cPP
Control
sEPSC cPP

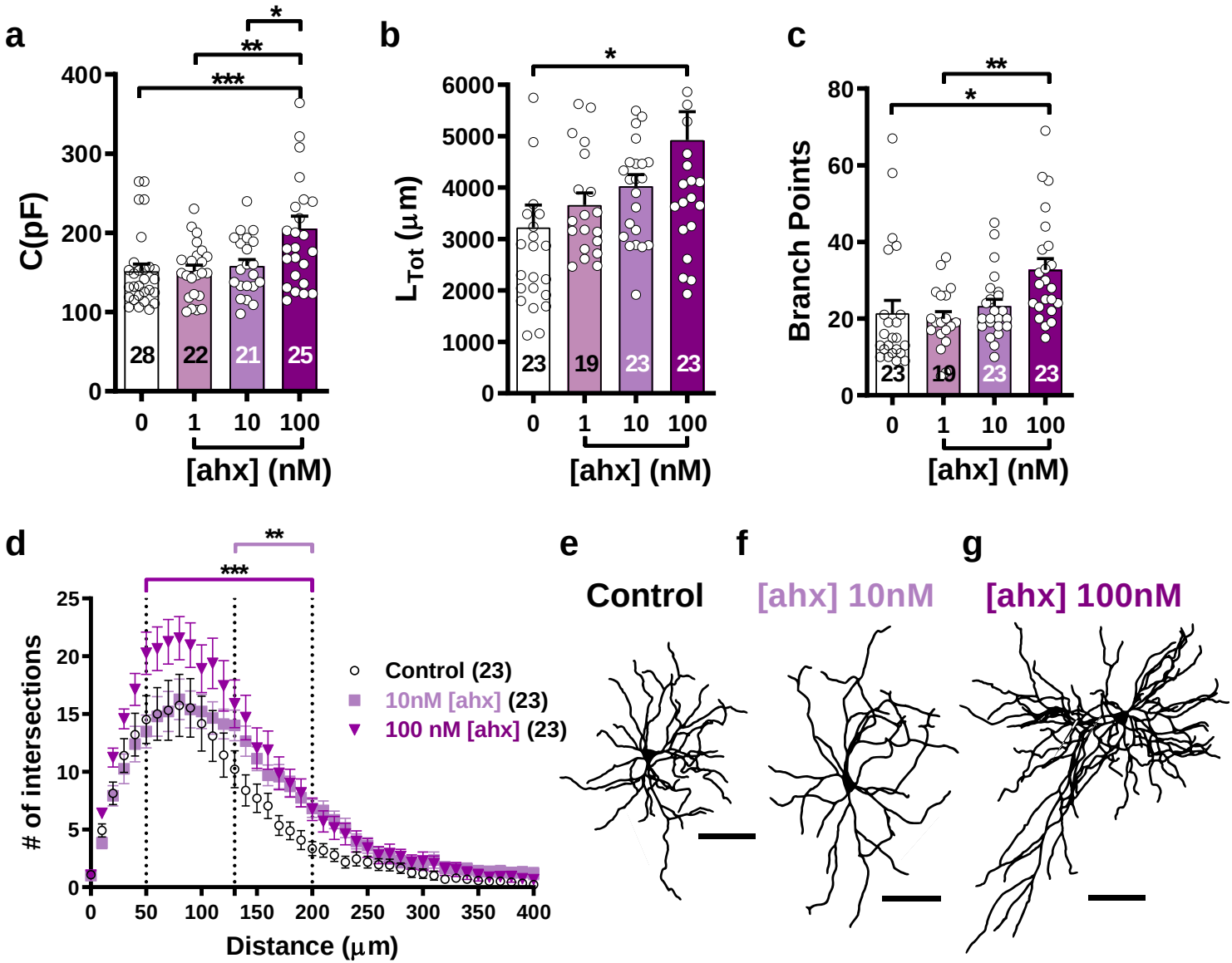
a
C(pF)
400
300
200
100
0
28
22
21
25
0
1
10
100
[ahx] (nM)
*
**
***
b
L_{Tot} (µm)
6000
5000
4000
3000
2000
1000
0
23
19
23
23
0
1
10
100
[ahx] (nM)
*
c
Branch Points
80
60
40
20
0
23
19
23
23
0
1
10
100
[ahx] (nM)
**
*
d
# of intersections
25
20
15
10
5
0
0
50
100
150
200
250
300
350
400
Distance (µm)
**
***
Control (23)
10nM [ahx] (23)
100 nM [ahx] (23)
e
Control
f
[ahx] 10nM
g
[ahx] 100nM

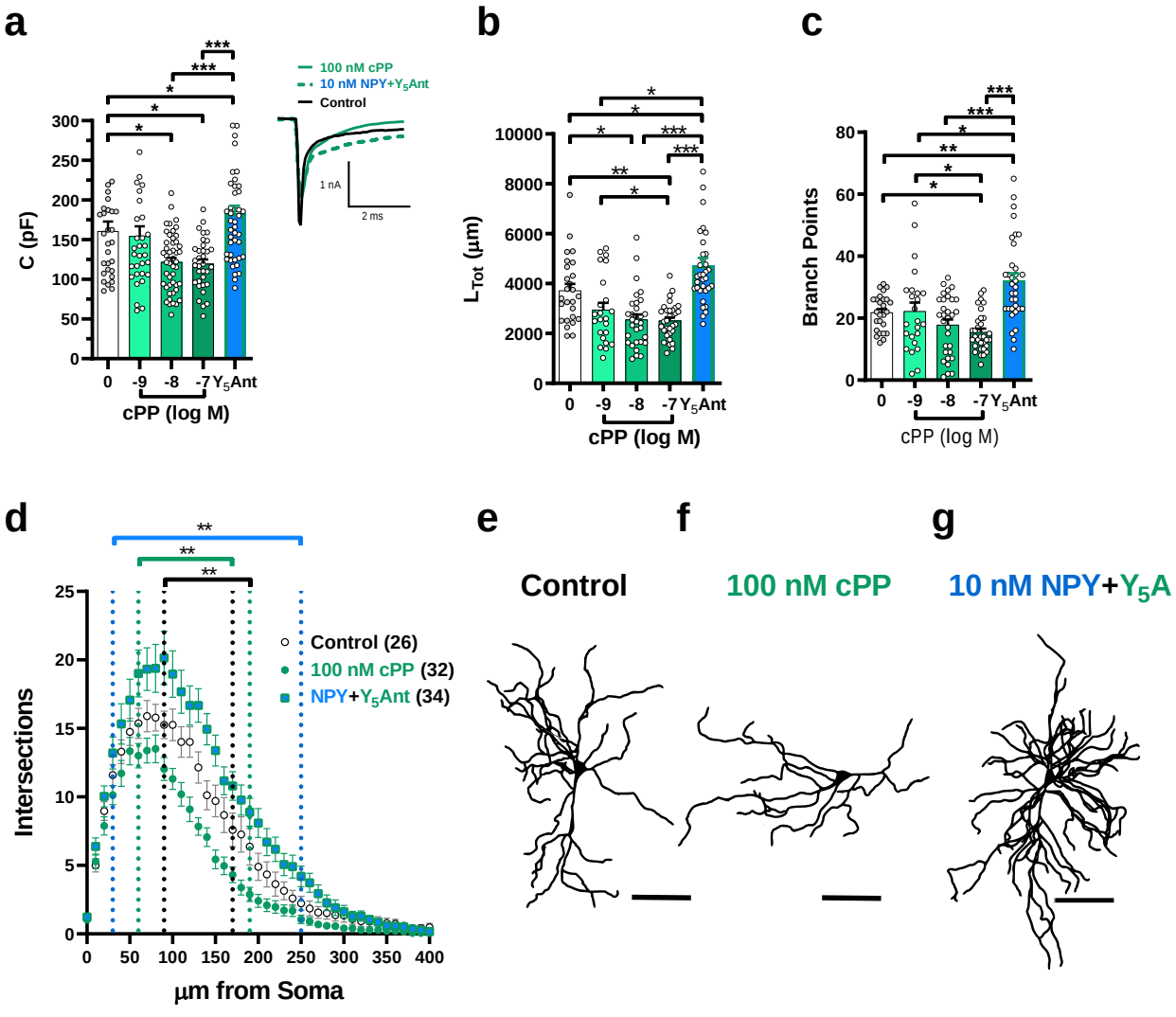
a
C (pF)
cPP (log M)
0
-9
-8
-7
Y5Ant
100 nM cPP
10 nM NPY+Y5Ant
Control
1 nA
2 ms
b
LTot (µm)
cPP (log M)
c
Branch Points
cPP (log M)
d
Intersections
µm from Soma
Control (26)
100 nM cPP (32)
NPY+Y5Ant (34)
e
Control
f
100 nM cPP
g
10 nM NPY+Y5A

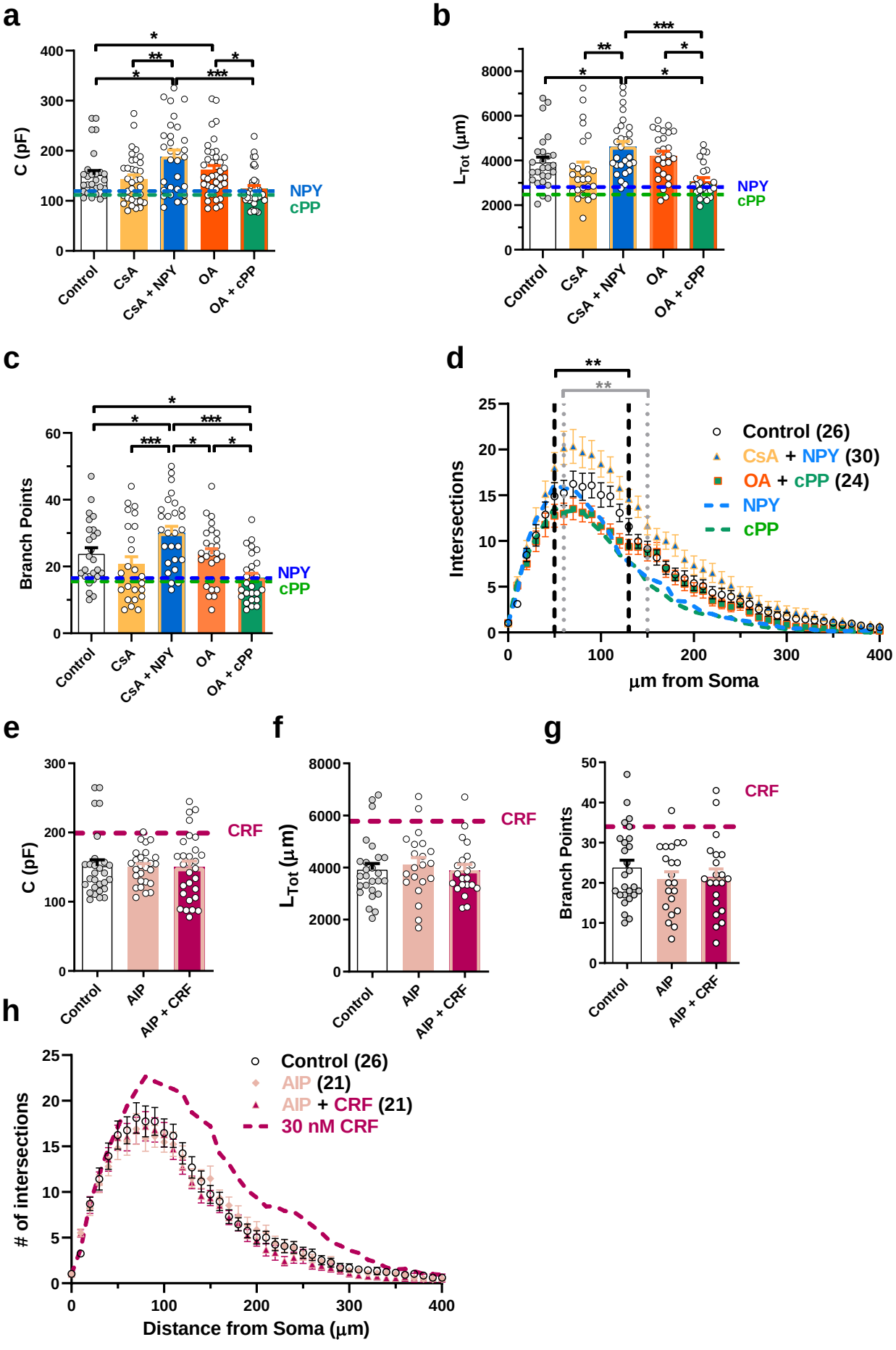
a
C (pF)
NPY
cPP
Control
CsA
CsA + NPY
OA
OA + cPP
b
L_{Tot} (µm)
c
Branch Points
d
Intersections
µm from Soma
Control (26)
CsA + NPY (30)
OA + cPP (24)
e
AIP
AIP + CRF
CRF
f
g
h
# of intersections
Distance from Soma (µm)
AIP (21)
AIP + CRF (21)
30 nM CRF

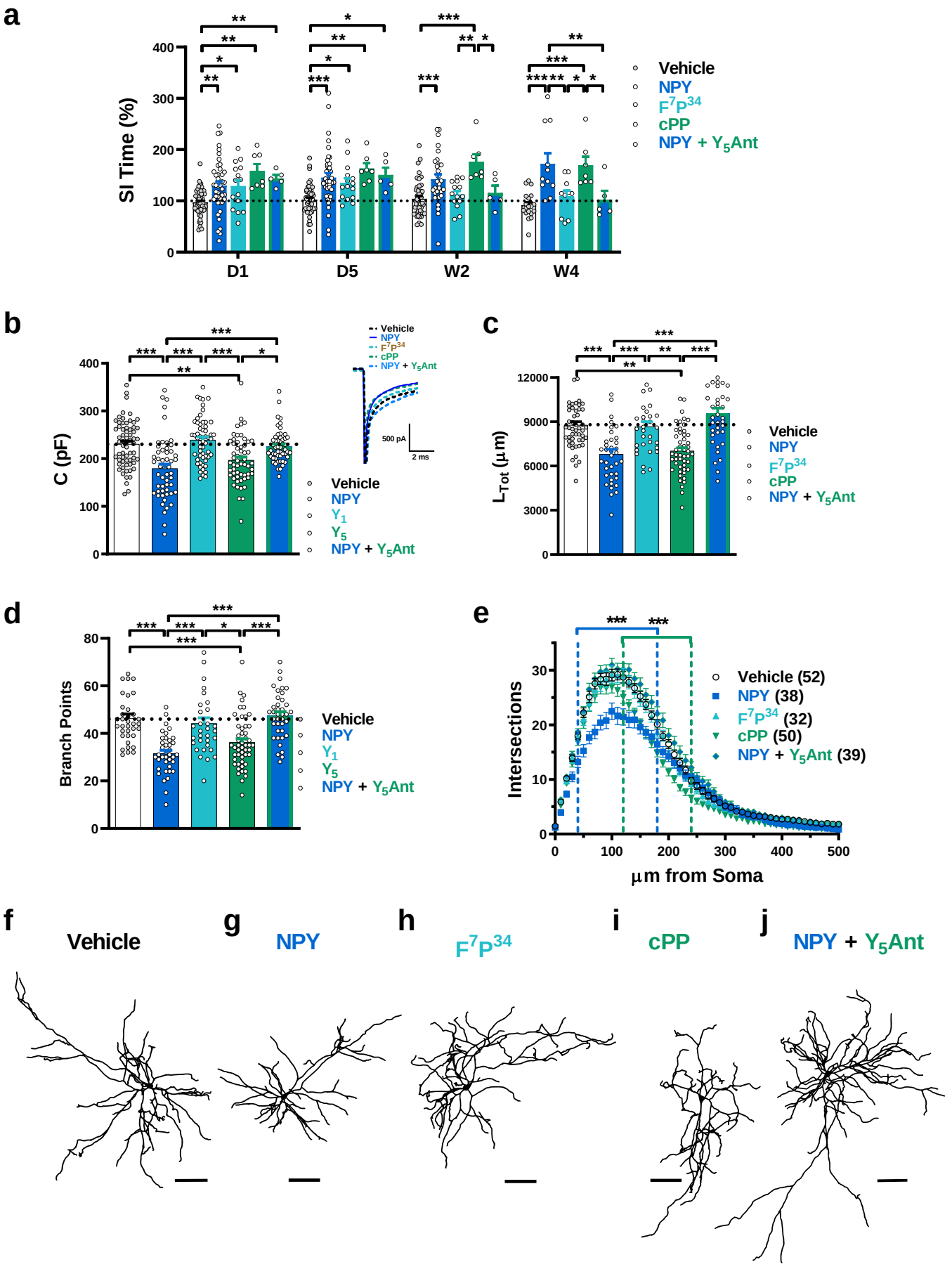
a
SI Time (%)
D1
D5
W2
W4
Vehicle
NPY
F7P34
cPP
NPY + Y5Ant
b
C (pF)
Vehicle
NPY
Y1
Y5
NPY + Y5Ant
500 pA
2 ms
c
LTot (µm)
d
Branch Points
e
Intersections
µm from Soma
Vehicle (52)
NPY (38)
F7P34 (32)
cPP (50)
NPY + Y5Ant (39)
f
Vehicle
g
NPY
h
F7P34
i
cPP
j
NPY + Y5Ant

a

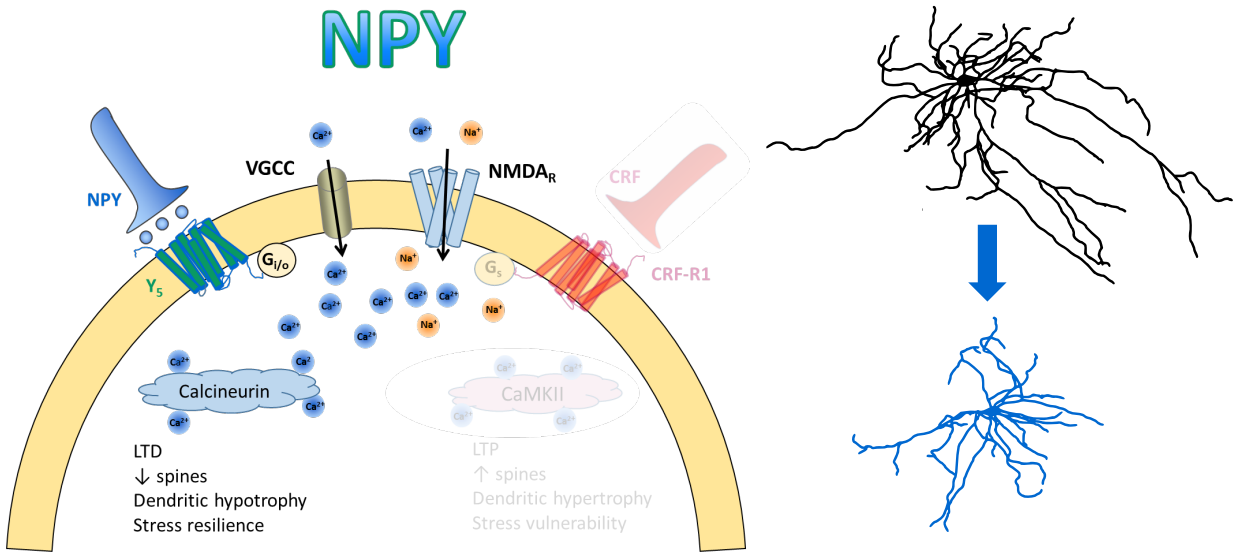
NPY
NPY
VGCC
NMDA$_R$
CRF
$G_{i/o}$
Y_5
G_s
CRF-R1
Calcineurin
CaMKII
LTD
↓ spines
Dendritic hypotrophy
Stress resilience
LTP
↑ spines
Dendritic hypertrophy
Stress vulnerability

b

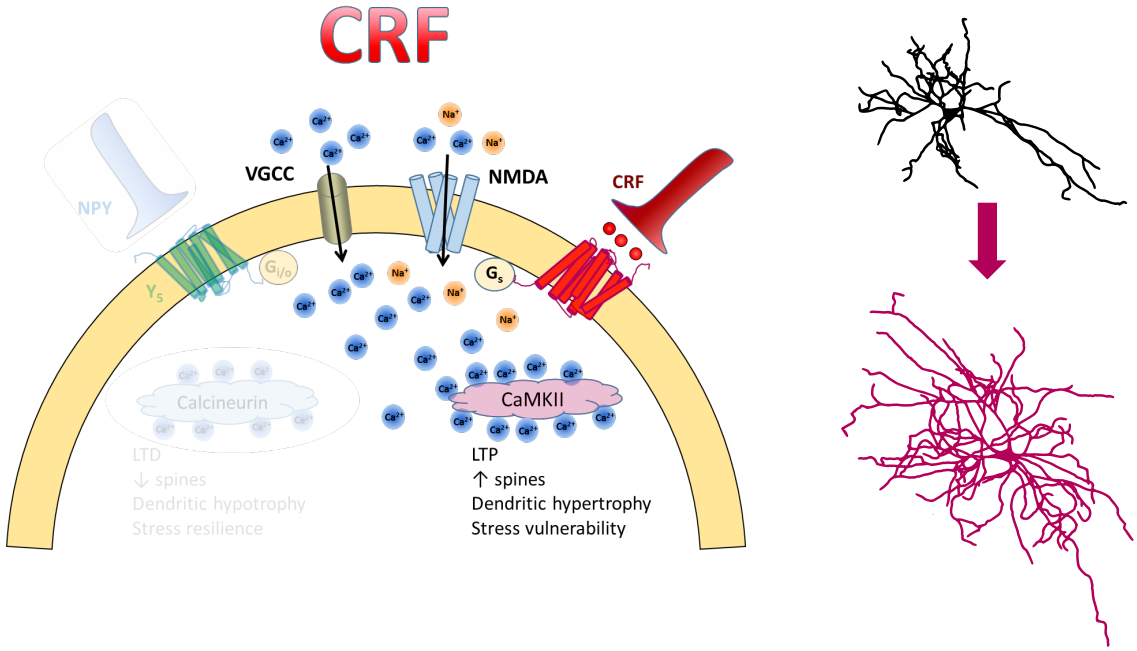
CRF
NPY
VGCC
NMDA
CRF
$G_{i/o}$
Y_5
G_s
Calcineurin
CaMKII
LTD
↓ spines
Dendritic hypotrophy
Stress resilience
LTP
↑ spines
Dendritic hypertrophy
Stress vulnerability

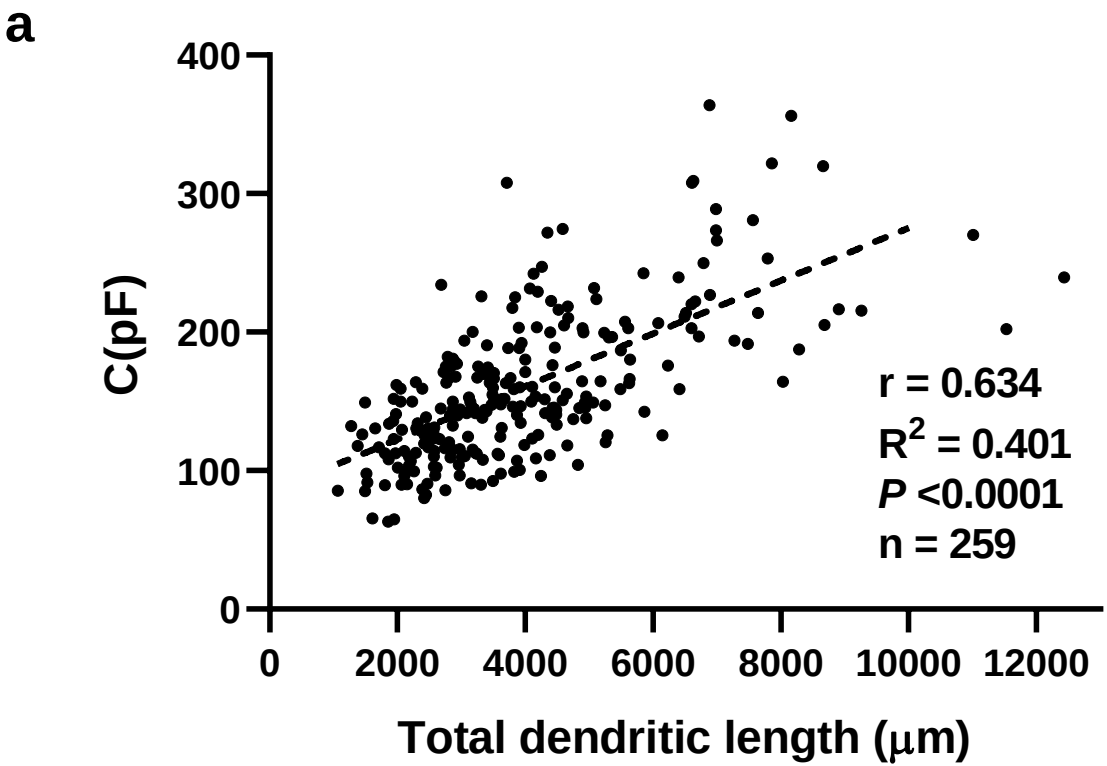
a
400
300
200
100
0
C(pF)
0
2000
4000
6000
8000
10000
12000
Total dendritic length (μm)
r = 0.634
R2 = 0.401
P <0.0001
n = 259